**Title**
Energy Analysis For Producing Low Carbon-footprint Cementitious Building Material



**Author**
Linden, Louis Zvi

**Publication Date**
2017

Peer reviewed|Thesis/dissertation

University of California
Los Angeles

# Energy Analysis For Producing Low Carbon-footprint Cementitious Building Material

A thesis submitted in partial satisfaction
of the requirements for the degree
Master of Science in Mechanical Engineering

by

Louis Zvi Linden

2017

# Abstract of the Thesis

Energy Analysis For Producing Low Carbon-footprint Cementitious Building Material

by

Louis Zvi Linden
Master of Science in Mechanical Engineering
University of California, Los Angeles, 2017
Professor Laurent G. Pilon, Chair

This thesis investigates the energy usage in the production processes of a low carbon-footprint building material called $CO_2$NCRETE. It consists of capturing carbon dioxide ($CO_2$) gas into limestone through the carbonation of three-dimensional printed portlandlite pre-formed structures. Carbonation can be enhanced by compressing and/or concentrating the $CO_2$ in the flue gas. Compression of the flue gas from atmospheric pressure to high pressure (3 MPa) results in high energy requirements for the building material production process. Consequently, the high energy requirements present an opportunity to investigate improvements into the reduction of net energy use. Hot flue gas ($\sim 150^o$C) emitted from coal-fired power plants can be used as an input into the $CO_2$NCRETE production process. An average coal-fired power plant producing 500 MW of electricity and emitting 700 kg/s of flue gas was used as a case study. In order to make the process energy efficient, two waste heat recovery systems were analyzed to provide power for the pressurized carbonation process. The first waste heat recovery system consists of an organic Rankine cycle using R245fa as a working fluid and operating between the flue gas at $150^o$C and a cold source at $20^o$C. It was found to generate 13.7 kW per MW generated by the coal-fired power plant power under maximum net power conditions. The second system consists of a transcritical Rankine cycle using $CO_2$ as a working fluid operating also between a hot source at $150^o$C and a cold source at $20^o$C. Under the same conditions, the transcritical Rankine cycle was found to generate 15.7 kW per MW generated by the coal-fired power plant. Finally, the compressed carbonation in $CO_2$NCRETE production was modeled at the lab scale. The compressed carbonation was

found to require 2,181 kg of flue gas, and produce 638 kg of $CO_2$NCRETE per day. The energy requirement was 1,589 kJ/kg of $CO_2$NCRETE. At this production rate, the waste heat recovery systems could provide 2.3% of the total energy required. However, the waste heat recovery systems will provide an increasing fraction of the energy necessary for compression as production rate and pressure are reduced.

The thesis of Louis Zvi Linden is approved.

Yongjie Hu

Adrienne G. Lavine

Laurent G. Pilon, Committee Chair

University of California, Los Angeles

2017

# Table of Contents

# List of Figures

# List of Tables

# Nomenclature

| | |
|---|---|
| $c_p$ | constant pressure specific heat, kJ/kg-K |
| $C$ | fraction of hydrated lime sample carbonated |
| $h$ | enthalpy, kJ/kg |
| $\dot{I}$ | rate of exergy destruction, kW |
| $m$ | mass, kg |
| $\dot{m}$ | mass flow rate, kg/s |
| $M$ | molar mass, kg/mol |
| $N$ | total amount of moles, mol |
| $n$ | moles per batch, mol |
| $P$ | pressure, MPa |
| $Q$ | heat, kW |
| $s$ | entropy, kJ/kg-K |
| $t$ | time, hr |
| $T$ | temperature, $^o$C |
| $V$ | volume, m$^3$ |
| $W$ | work, kJ |
| $\dot{W}$ | power, kW |
| $y$ | mole fraction |
| $Z$ | compressibility factor |

**Greek symbols**

| | |
|---|---|
| $\Delta T$ | pinch point temperature difference |
| $\eta_{th}$ | thermal efficiency |
| $\eta_I$ | Carnot efficiency |
| $\eta_{II}$ | second law efficiency |
| $\eta_s$ | isentropic efficiency |
| $\dot{\Psi}$ | exergy flow rate, kW |

**Subscripts**

| | |
|---|---|
| 1 | refers to the first carbonation/compression stage |
| 2 | refers to the second carbonation/compression stage |
| $a$ | refers to an arbitrary component in a Rankine cycle |
| $C$ | refers to the cold source |
| $w$ | refers to cooling water |
| $CL$ | refers to carbonated lime, $CaCO_3$ |
| $CO_2$ | refers to the carbon dioxide constituent of a mixture |
| $crit$ | refers to the critical state of a fluid |
| $e$ | refers to the exit |
| $g$ | refers to power plant flue gas |
| $H$ | refers to the hot source |
| $H_2O$ | refers to the water constituent of a mixture |
| $i$ | refers to the inlet |
| $in$ | refers to the quantity added to the system |
| $j$ | refers to an arbitrary state |
| $mix$ | refers to the entire mixture of a gas |
| $N_2$ | refers to the nitrogen constituent of a mixture |
| $net$ | refers to the net quantity |
| $O_2$ | refers to the oxygen constituent of a mixture |
| $out$ | refers to the quantity removed from the system |
| $R$ | refers to the reduced value |
| $s$ | refers to an isentropic process |
| $tot$ | refers to the total |

# CHAPTER 1

# Introduction

Flue gas emitted from coal-fired power plants accounts for 1,600 million metric tons of $CO_2$ emissions per year, or 28% of annual $CO_2$ emissions in the United States [1,6]. This flue gas is typically released to the atmosphere at temperatures near $150^oC$ [7–9]. Given the large volume and relatively high temperature of this waste heat stream, coal-fired power plant flue gas is a potentially large source of low grade thermal energy [5].

Numerous technologies exist to convert waste heat into electricity including thermoelectric systems [10], Kalina cycles [4], organic Rankine cycles (ORCs) [5], and transcritical Rankine cycles (TRCs) [11]. Organic Rankine cycles subject organic fluids (e.g., alcohols) to identical processes to conventional steam Rankine cycles, albeit at a lower boiling point, Transcritical Rankine cycles are conventional Rankine cycles in which heating of the working fluid occurs at a supercritical state. They have been considered as an alternative to ORCs [11–16].

The manufacturing of cement, an input for concrete which is widely used as a building material, accounts for 5-7% of global $CO_2$ emissions [17]. However, $CO_2$ in the atmosphere is naturally absorbed by concrete structures over their lifetime [18]. This phenomena is known as carbonation and can have significant effects on the level of $CO_2$ in the atmosphere [19,20]. The effectiveness of carbonation by concrete structures, however, is limited due to the surfacial nature of the chemical reaction [20]. A chemical process has been proposed in which carbonation occurs during the production of the building material using high pressure $CO_2$ [21]. This method can provide a larger amount of $CO_2$ sequestration than carbonation occurring post-production, resulting in a low carbon-footprint cementitious building material.

Therefore, the use of coal-fired power plant flue gas presents an opportunity to both

capture low-grade thermal energy through waste heat to power systems as well as mitigate $CO_2$ emissions that occur as a result of cementitious building material production.

## 1.1 Main sources of $CO_2$ emissions

### 1.1.1 Power plants

In 2014, 2000 metric tons or 37% of overall U.S. $CO_2$ emissions were the result of electricity generation [6]. Table 1.1 shows the distribution of electricity generation and $CO_2$ emissions by fuel source for the U.S. in 2014. Coal-fired power plants accounted for the largest portion of both electricity generation and $CO_2$ emissions. In fact, they accounted for 39% of all electricity generation but also contributed 76% to the $CO_2$ emissions [1]. On the other hand, natural gas produced 27% of annual electricity generation and was responsible for 22% of power plant $CO_2$ emissions [1].

Table 1.1: Annual electricity generation and $CO_2$ emissions by fuel source in the U.S. in 2014 [1].

| **Source** | **Electricity generation** | **$CO_2$ emissions** | |
|---|---|---|---|
| | % of total | Million metric tons | % of total |
| Coal | 39% | 1,562 | 76% |
| Nuclear and renewables | 33% | 11 | 1% |
| Natural gas | 27% | 444 | 22% |
| Petroleum | 1% | 23 | 1% |
| Total | 100% | 2,043 | 100% |

In order to limit pollutant emissions and recover some of the flue gas residual thermal energy, flue gas undergoes several processes. Figure 1.1 illustrates these different processes. Thermal energy in the hot flue gas leaving the boiler is typically recovered by the economizer followed by an air preheater (APH). Flue gas heat recovery in the APH is performed until the flue gas temperature drops to about 150$^o$C (depending on the type of coal consumed) to prevent $H_2SO_4$ from condensing on the APH surface and downstream ducts/systems [22–24].

Indeed, cooling of the flue gas below the acid dew point can lead to acid condensation and deposition which in turn can cause corrosion and fouling in the downstream ducts and equipment [25]. Such fouling and plugging result in increasing pressure drop and power consumption to force the flue gas through the APH. This acid dewpoint can be as high as 140$^o$C [26–28]. Acid dewpoint as well the amount of pollutants are determined primarily by the flue gas composition.

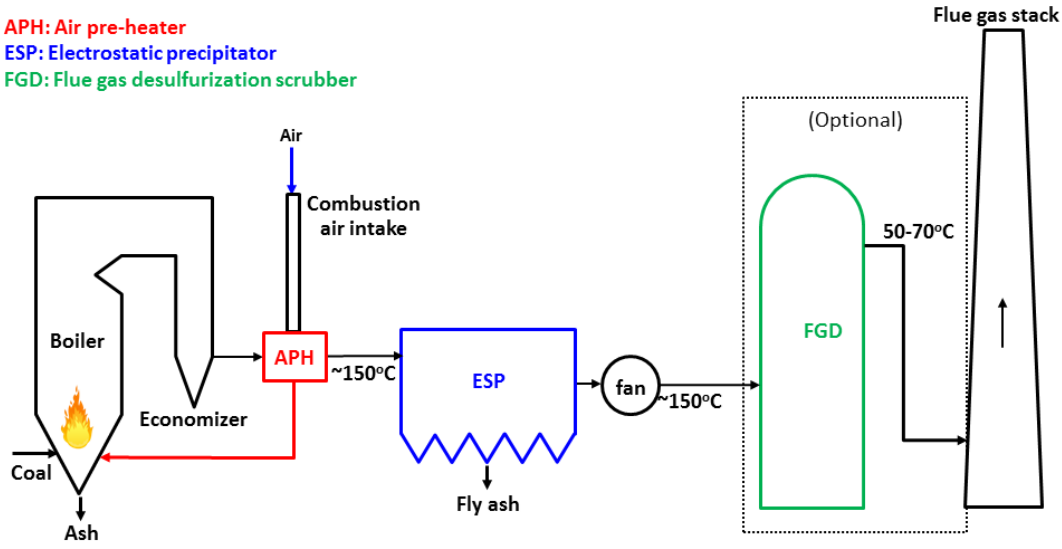


Figure 1.1: An illustration of the flue gas path in a coal-fired power plant.

Finally, the flue gas leaving the electrostatic precipitator at around 150-170$^o$C may be injected with activated carbon to remove Hg traces before entering the flue gas desulfurization (FGD) system [29,30]. About 85% of FGD systems in the U.S. are wet systems consisting of a spray tower in which the flue gas contacts a mist of droplets of aqueous slurry of sorbent particles such as hydrated lime ($Ca(OH)_2$) and limestone ($CaCO_3$) [31]. Water evaporation reduces the flue gas temperature to 50-to-70$^o$C at which the desulfurization process is most efficient [32–34]. The sorbent particles react with $SO_2$ in the flue gas to form insoluble calcium sulfite ($CaSO_3$) which reacts with oxygen to produce gypsum. This way, 95% of the $SO_2$ is removed from the stream [35].

An alternative to removing sulfur after combustion in FGD systems consists of burning low sulphur-content coal to meet emissions standards. Both bituminous and subbituminous

coals, which make up over 90% of U.S. coal mining production, can be considered low sulfur [36]. Low sulfur coal deposits are primarily found in the western U.S., especially in Montana [37, 38].

Alternatively, coal can be cleaned to reduce its sulfur content prior to combustion [37]. This typically starts with crushing the coal into small particles. Then, jets of water cause the lighter coal particles to rise and heavier impurities to sink to the bottom. Finally, the coal particles are filtered through mechanical screening and thermal drying [39].

In 2010, 40% of electricity generation from coal-fired power plants did not undergo flue gas desulphurization [40]. In this case, flue gas temperature at the stack was typically around 150$^o$C [7, 8]. In fact, 25% of coal-fired power plant stacks have been reported to have a temperature of 150$^o$C or greater [9].

Table 1.2 summarizes the flue gas composition for typical coal-fired and gas-fired power plants on a volume basis. Flue gas from coal-fired power plants consists of 12.6 vol.% $CO_2$, nearly twice that of gas-fired power plants at 7.5 vol.% [2]. From a molar mass analysis, the $CO_2$ composition by weight can be found to be 18.9 wt.% for a coal-fired power plant and 12.1 wt.% $CO_2$ for a gas-fired plant.

Table 1.2: Flue gas composition of coal-fired and gas-fired power plant flue gas on a volume basis [2].

| **(% vol.)** | Coal-fired | Gas-fired |
|---|---|---|
| **$CO_2$** | 12.60% | 7.7% |
| **$H_2O$** | 6.20% | 14.60% |
| **$O_2$** | 4.40% | 4.45% |
| **CO** | 50 ppm | 250 ppm |
| **$NO_x$** | 420 ppm | 60-70 ppm |
| **$SO_2$** | 420 ppm | 0 |
| **$N_2$** | 76% | 73.2% |

As a result of the high concentration of $CO_2$ in coal-fired power plants, approximately

950 kg of $CO_2$ are released per MWh by a coal-fired power plant [41]. This is equivalent to 0.26 kg/s of $CO_2$ and 1.4 kg/s of flue gas per MW.

### 1.1.2 Cement production

Cement manufacturing accounts for 5-7% of global $CO_2$ emissions [17]. For each kilogram of cement produced, 0.9 kg of $CO_2$ is released into the atmosphere [17]. The high level of cement-related $CO_2$ emissions is caused primarily by three factors. *First*, cement is used to make concrete which is ubiquitously used as a building material for roads and buildings, for example. In 2014, 80 million tons of cement were produced in the U.S. alone. Most of it was used for concrete production [42]. *Second*, cement production releases a large amount of $CO_2$ due to an energy intensive production process. After grinding and mixing raw materials including limestone, magnesium carbonate, silica, alumina and iron oxide, the mix is sent to a preheater [17]. Next, the mix is sent to a kiln where it undergoes a process known as clinkering. Clinkering consists of melting the different constituent materials together at temperatures as high as $1450^oC$ [17, 43]. Combustion of large amounts of fossil fuels is required to maintain these temperatures and contributes to $CO_2$ emisssions. *Third*, cement production releases large amounts of carbon dioxide as the result of the chemical decomposition of lime, according to the chemical formula [44],

$$CaCO_3 \xrightarrow{heat} CaO + CO_2, \tag{1.1}$$

where $CaCO_3$ is calcium carbonate (commonly known as limestone) and CaO is calcium oxide (commonly known as quicklime). A similar decomposition reaction occurs with magnesium carbonate ($MgCO_3$). However, magnesium oxide (MgO), the product of decomposition of magnesium carbonate, represents a relatively small portion of typical cement composition, (0.5-2% by weight compared to 40% for quicklime) [17]. It is estimated that 50% of $CO_2$ emitted from cement manufacturing is a result of this decomposition reaction [17]. Flue gas from cement kilns can contain as much as 26% by weight of $CO_2$ [45].

## 1.2 $CO_2$NCRETE production processes

In order to mitigate the large greenhouse gas emissions of cement manufacturing, a novel low carbon-footprint cementitious building material production process has been proposed, termed the $CO_2$NCRETE production process [46]. Figure 1.2 shows a flow diagram of this production process. It consists of two streams, namely (i) a base material stream and (ii) a gas stream. First, the base material stream, consisting of lime, is mixed with water to create a lime slurry according to the reaction [46],

$$CaO + H_2O \rightarrow Ca(OH)_2. \tag{1.2}$$

where $Ca(OH)_2$ is hydyrated lime, or portlandite. This lime slurry is then mixed with aggregates and formed into a monolith with the desired three-dimensional (3D) shape by additive manufacturing (or 3D printing) which then reacts with the gas stream. In the gas stream, hot flue gas is diverted from a source such as a power plant. Heat from the flue gas is recovered in order to improve the energy efficiency of the process. A portion of the cold, dehumidified flue gas is then sent through a membrane to increase the $CO_2$ content of the gas stream, filtering out undesirable gases except for a portion of $N_2$ and $CO_2$. Then, the $CO_2$ enriched and un-enriched flue gas streams are compressed and sent into the carbonation chamber containing the printed monolith. Carbonation of the portlandite-containing monolith occurs according to the reaction [21],

$$Ca(OH)_2 + CO_2 \xrightarrow{water} CaCO_3 + H_2O. \tag{1.3}$$

## 1.3 Waste heat energy harvesting

It is common for heat to be released to the environment as a by-product of industrial processes such as cement manufacturing. This waste heat could be converted into electricity to increase the overall efficiency of the processes provided it can be performed at a reasonable cost. ICF International [5] estimates that the U.S. produces 766 MW of electricity from waste heat, but has the potential to produce 15,500 MW. This would represent 1.5% of the total electricity generation of the U.S., estimated as 1,000,000 MW [47].

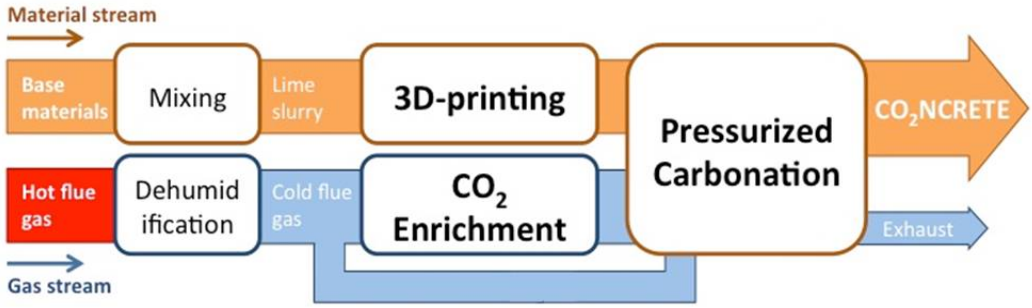


Figure 1.2: Flow diagram of production processes for $CO_2$NCRETE, a low carbon-footprint building material.

### 1.3.1 Waste heat energy harvesting technologies

Several waste heat energy harvesting technologies exist to convert waste heat directly or indirectly into electricity. Thermophotovoltaic generation systems passively convert infrared radiation emitted by heat sources directly into electricity using semi-conducting materials (e.g., Ge, GaSb, InGaAs). They have few moving parts but are typically restricted to temperatures above 800$^o$C in order for emitted photons to have energy larger than the bandgap of the thermophotovoltaic material [48]. Thermoelectric generation - based on the Seebeck effect - can be viable for waste heat energy conversion. It directly converts waste heat into electricity without any moving parts. A wide range of materials are available depending on the waste heat temperature range [10]. However, their efficiency is typically low and they have remained an order of magnitude more costly than other options [5, 10].

Table 1.3 categorizes more established waste heat to power technologies. Steam Rankine cycles have high thermal efficiencies above 450$^o$C but the efficiency drops significantly as the temperature decreases [3, 4]. Kalina cycles constist of performing a Rankine cycle on a mixture of two fluids with different boiling temperatures (e.g., ammonia and water). They can operate between 100 and 550$^o$C. However, their complexity prohibits small-scale systems and leads to higher cost [4, 5]. Organic Rankine cycles (ORCs) also perform the Rankine cycle, but on an organic working fluid. ORCs have been demonstrated with bench tests [49–54] and proven to be economically feasible at commercial scale [5, 55]. They are suitable

for heat resource temperatures near 150$^o$C corresponding to flue gas temperature [3–5]. Based on this information the organic Rankine cycle is a pragmatic choice for lab scale testing of heat recovery of a 150$^o$C waste heat stream. However, the Kalina cycle could more the appropriate choice at the commercial scale.

Table 1.3: Comparison of waste heat to power technologies [3–5].

| Technology | Cycle | Fluid | Temperature range | Typical capacity | Key facts |
|---|---|---|---|---|---|
| **Traditional steam cycle** | Rankine | Water | >500$^o$F >260$^o$C | Large (>10 MW) | Most efficient at higher temperatures |
| **Organic Rankine cycle** | Rankine | Organic fluid (i.e. R11, R245fa, etc.) | 200 - 500$^o$F 93 - 260$^o$C | Small to Medium (<10 MW) | Small sized units, air-cooled condensers, high availability |
| **Kalina cycle** | Rankine | Mixture with different boiling points (e.g., ammonia & water) | 200 - 1000$^o$F 93 - 538$^o$C | Medium (> 1 MW) | Highest theoretical efficiency, complex and new technology |

### 1.3.2 Principles of organic Rankine cycles

Figure 1.3 visualizes the elements required to perform the Rankine cycle processes. These elements are, a working fluid, hot source, cold source and four mechanical components, namely a pump, an evaporator, a turbine, and a condenser. The basic Rankine cycle consists of four thermodynamic processes: (1) reversible, adiabatic expansion of the working fluid through the turbine, (2) constant pressure heat transfer from the working fluid to a cold source in the condenser, (3) reversible adiabatic compression through the pump, and (4) constant pressure heat transfer from the hot source to the working fluid in the evaporator. Figure 1.4 plots the Rankine cycle processes on a (a) $P$-$v$ and (b) $T$-$s$ diagram for an arbitrary organic working fluid.

Thermal efficiency is often used as a metric to analyze how well thermodynamic cycles convert thermal energy into useful energy. Carnot efficiency, denoted by $\eta_{Carnot}$, defines the maximum thermal efficiency of any thermodynamic cycle between a hot source at temperature $T_H$ and a cold source at temperature $T_C$. It is defined as [56]

$$\eta_{Carnot} = 1 - \frac{T_C}{T_H}. \tag{1.4}$$

For example, the Carnot efficiency of a flue gas stream at 150$^o$C and a cold source of 20$^o$C

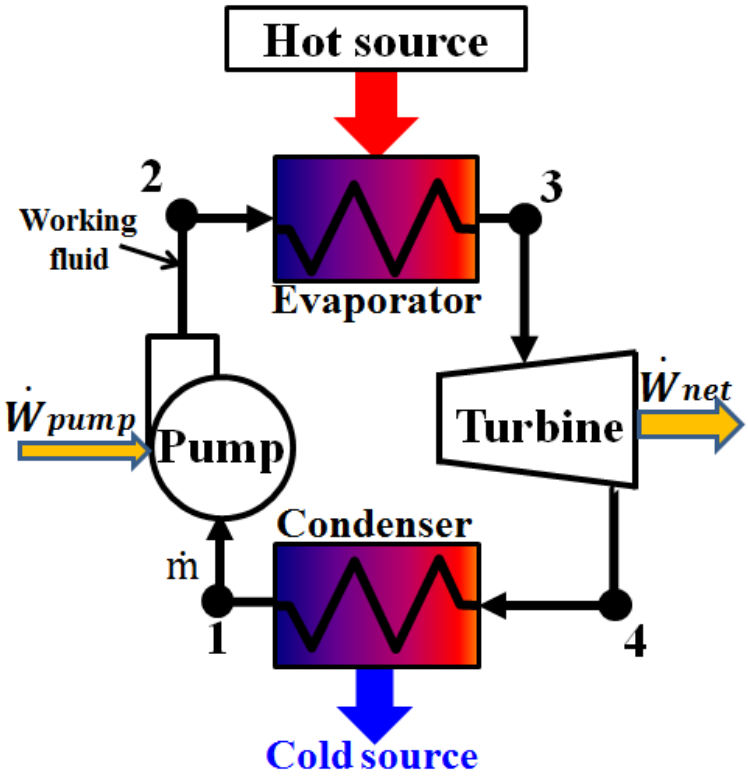


Figure 1.3: A visual representation of the elements and processes of a basic Rankine cycle.

is 31%. Figure 1.5 shows the Carnot efficiency as a function of hot source temperature $T_H$ for cold source temperature $T_C$ equal to 0$^o$C, 20$^o$C, and 50$^o$C.

Although the temperatures of the hot and cold sources are important parameters, the working fluid is another key factor in designing a Rankine cycle. Several properties of fluids are used to determine the optimal working fluid such as (i) boiling and condensing temperatures and pressures, (ii) global warming potential, and (iii) the phase of saturated vapor under reversible adiabatic, or isentropic processes [57]. For example, organic fluids often have low boiling and condensing temperatures making them ideal for low grade waste heat recovery applications [58, 59]. Additionally, many organic fluids are dry, meaning the fluid is at a superheated vapor state under isentropic expansion from a saturated vapor state [60]. This property of dry fluids is of note because a superheated state at the exit of the turbine prevents corrosion and damage [61].

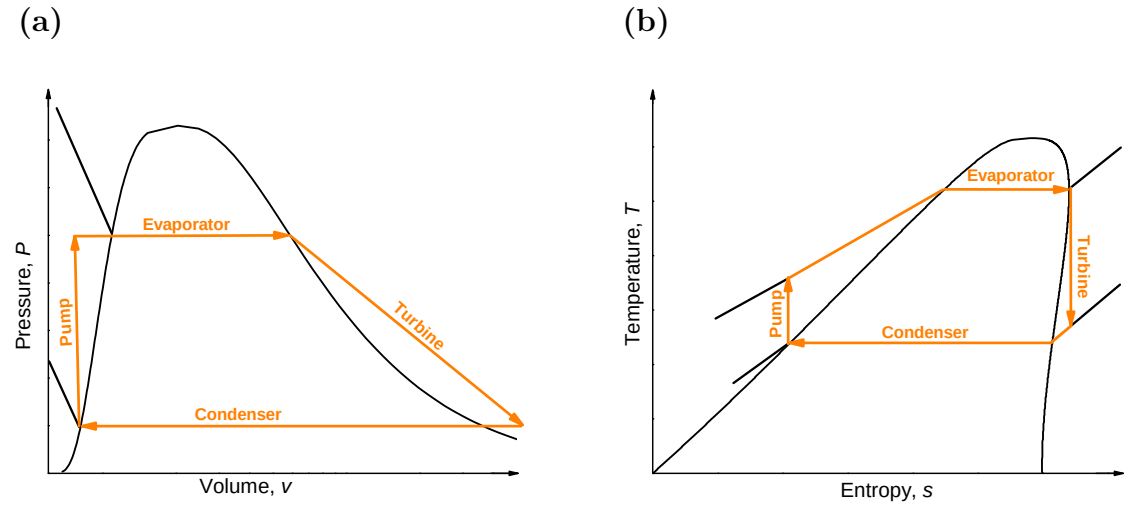


Figure 1.4: A (a) $P$-$v$ and (b) $T$-$s$ diagram of an arbitrary organic Rankine cycle.

### 1.3.3 Transcritical Rankine cycles

Transcritical Rankine cycles (TRCs) have been considered as an alternative to conventional organic Rankine cycles [11–16]. While TRCs consist of identical elements as ORCs (Figure 1.3), TRCs feature a heating process in the evaporator[1] during which the working fluid is in a supercritical state, i.e., its temperature and pressure are above that of the critical point [62]. The critical point occurs at the critical temperature and critical pressure, where the saturated liquid and saturated vapor states are identical, as illustrated in Figure 1.6 [62]. Figure 1.6 also plots the transcritical Rankine cycle processes in a $P$-$v$ and $T$-$s$ diagram.

Transcritical cycles feature a lower average temperature difference between the heat source and the working fluid due to changing temperature in the evaporator. To illustrate the advantage of the TRC over the ORC, consider two cases illustrated in Figure 1.7. Case 1 corresponds to a conventional Rankine cycle in which single-phase heat transfer prevails in the hot source stream and two-phase heat transfer occurs in the working fluid stream in the evaporator. Case 2 corresponds to a TRC in which single-phase heat transfer prevails in

[1]Although no evaporation takes place in the transcritical cycle, the heat exchanger where the fluid in a transcritical cycle is heated will be referred to as the evaporator for the sake of convenience.

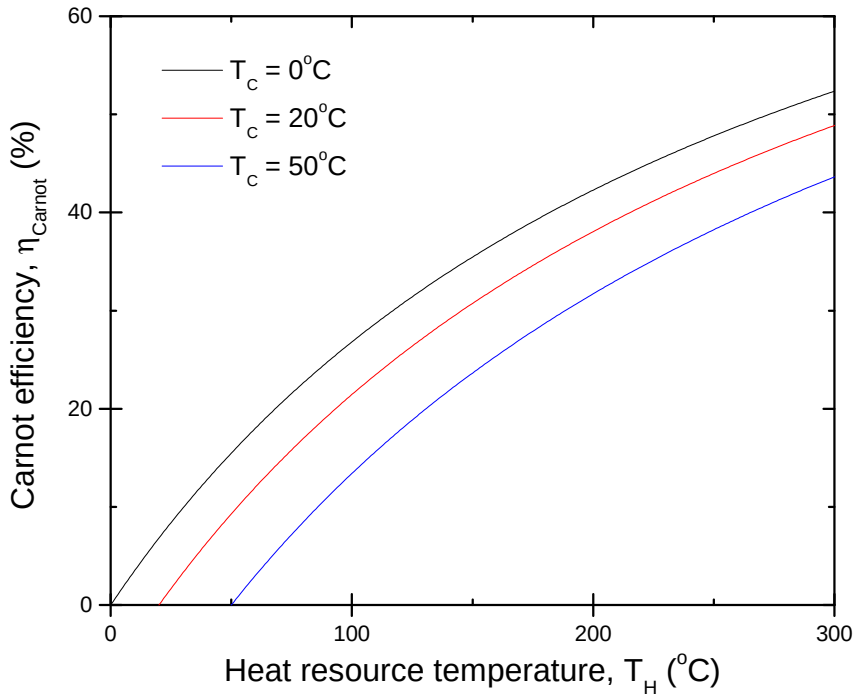


Figure 1.5: Carnot efficiency $\eta_{Carnot}$ as a function of hot source temperature, $T_H$, for heat sink temperatures $T_C = 0^o$C, $20^o$C, and $50^o$C.

both the hot source and working fluid streams in the evaporator. For Case 1, the minimum temperature difference, commonly known as the pinch point temperature difference [61], often occurs when a fluid is a saturated liquid. However, in Case 2 the pinch point occurs at the inlet or exit points of the hot source or working fluid, depending on the relative products of mass flow rate and specific heat capacity of each fluid. As a result of the smaller average temperature difference between the working fluid and hot source streams, TRCs tend to feature less entropy generation [11].

## 1.4 Objectives of the study

A novel low carbon-footprint building material production process has been developed to upcycle the $CO_2$ emitted in the flue gas of various industrial processes. This present study

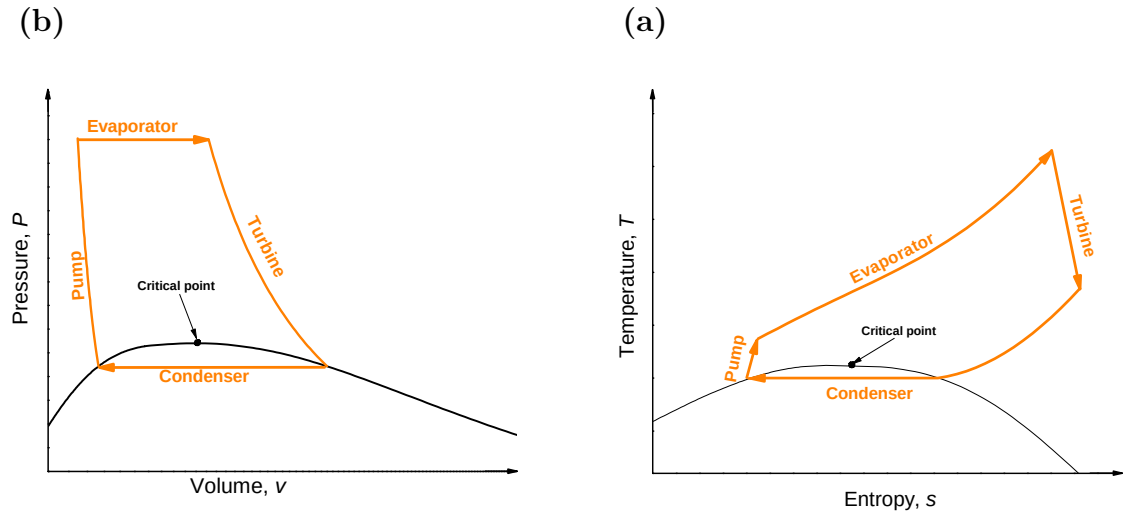


Figure 1.6: A (a) $P$-$v$ and (b) $T$-$s$ diagram of an arbitrary transcritical Rankine cycle.

specifically considers an ORC and a TRC for the performance of waste heat recovery from hot flue gas exiting coal-fired power plants. In addition, the building material production process was modeled and its energy requirements were evaluated in order to determine the performance and feasibility of the waste heat recovery systems.

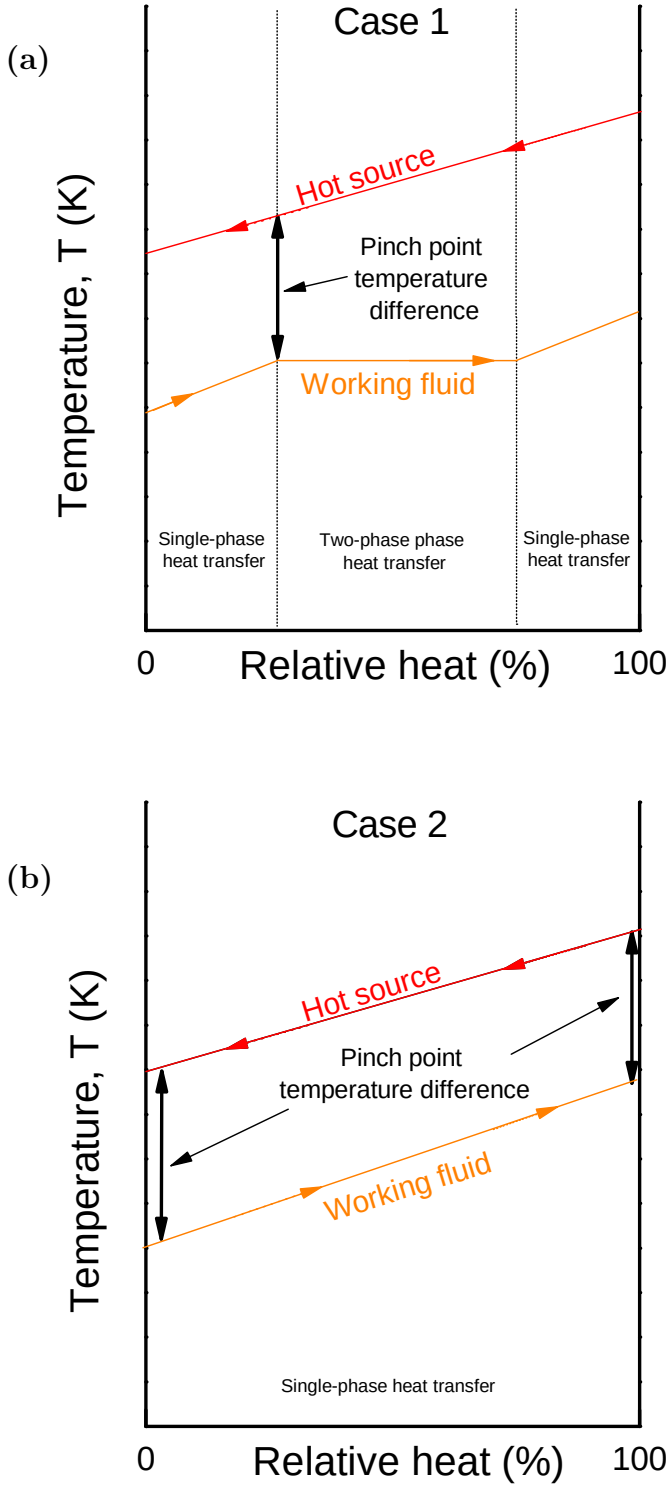


Figure 1.7: Diagrams of pinch point locations in (a) two-phase and (b) single-phase heat transfer in the evaporator.

# CHAPTER 2

# Waste heat harvesting by Rankine cycles

## 2.1 Introduction

Coal-fired power plants release flue gas at temperatures near 150$^o$C and the $CO_2$NCRETE production process uses $CO_2$ as an input for carbonation of lime. In this chapter, a waste heat recovery system was considered to improve the energy efficiency of $CO_2$NCRETE production. Both an organic Rankine cycle (Section 1.3.2) and transcritical Rankine cycle (Section 1.3.3) were considered for waste heat recovery of the hot flue gas.

## 2.2 Analysis

### 2.2.1 Schematic and phase diagrams

#### 2.2.1.1 Organic Rankine cycle

The ORC investigated in this study uses (i) of 1,1,1,3,3-Pentafluoropropane (R245fa) as the working fluid, (ii) power plant flue gas as a hot source at 150$^o$C, and (iii) water as a cold source at 20$^o$C. R245fa was chosen for several reasons. As a dry fluid, the consideration of R245fa vapor condensation in the turbine is non-existent. Additionally, Wang et al. [63] found that when safety and environmental properties are considered (including the ASHRAE 34 safety group, atmospheric life time, ozone depletion potential, and global warming potential), R245fa is one of two working fluids most suitable for engine waste-heat recovery at a hot source temperature ranging from $27-327^o$C. Similarly, Lakew and Bolland [64] recommended R245fa for waste heat sources in the temperature range of 160-200$^o$C. Additionally, R245fa

has been proven to be cost-effective at commercial scale in many commercial ORC systems [55]. Further, unlike many other organic fluids R245fa, has been the subject of bench tests for the operation of individual mechanical components [65–67] and full cycle operation [49, 51, 53]. Laboratory operation of pumps and turbines can be difficult, especially because these components are often highly sensitive to the type of working fluid [49, 55, 67]. Therefore, previous demonstration of bench operation of ORCs with R245fa as a working fluid will significantly contribute to easier set-up and operation for a newly built ORC system.

Figure 2.1 plots the Rankine cycle in the $T$-$s$ diagram for R245fa as the working fluid. It also plots the temperature of the hot flue gas entering at $T_{g,i} = 150^o$C and exiting at $T_{g,e}$. Similarly, the cold water enters at $T_{w,i} = 20^o$C and exits at $T_{w,e}$. Subscripts "$i$" and "$e$" refer to the inlet and exit of the cold source and hot source lines. For the flue gas and cooling water, the location of the pinch point temperature difference is denoted by the subscript $P$. The pinch point temperature difference refers to states where the temperature difference between either flue gas and R245fa, or cooling water and R245fa, is the smallest. For the working fluid the location of the pinch point temperature difference is denoted by a quotation mark " $'$ ".

#### 2.2.1.2 Transcritical Rankine cycle

In this study, we also consider a transcritical Rankine cycle performed on $CO_2$ as the working fluid. $CO_2$ was chosen as the working fluid because it is (i) non-toxic [68], (ii) non-flammable [68, 69], (iii) inexpensive [15], (iv) has well-defined thermodynamic properties in the supercritical region [16], and (v) a critical point at moderate temperature and pressure ($31^o$C, 7.4 MPa).

Figure 2.2 shows a TRC performed in the $CO_2$ $T$-$s$ phase diagram between a hot source at $T_{g,i} = 150^o$C and a cold source at $T_{w,i} = 20^o$C. The variables representing each state were defined identical to those in Figure 2.1, except the flue gas inlet $T_{g,i}$ is equivalent to the location of the flue gas pinch point $T_{g,P}$.

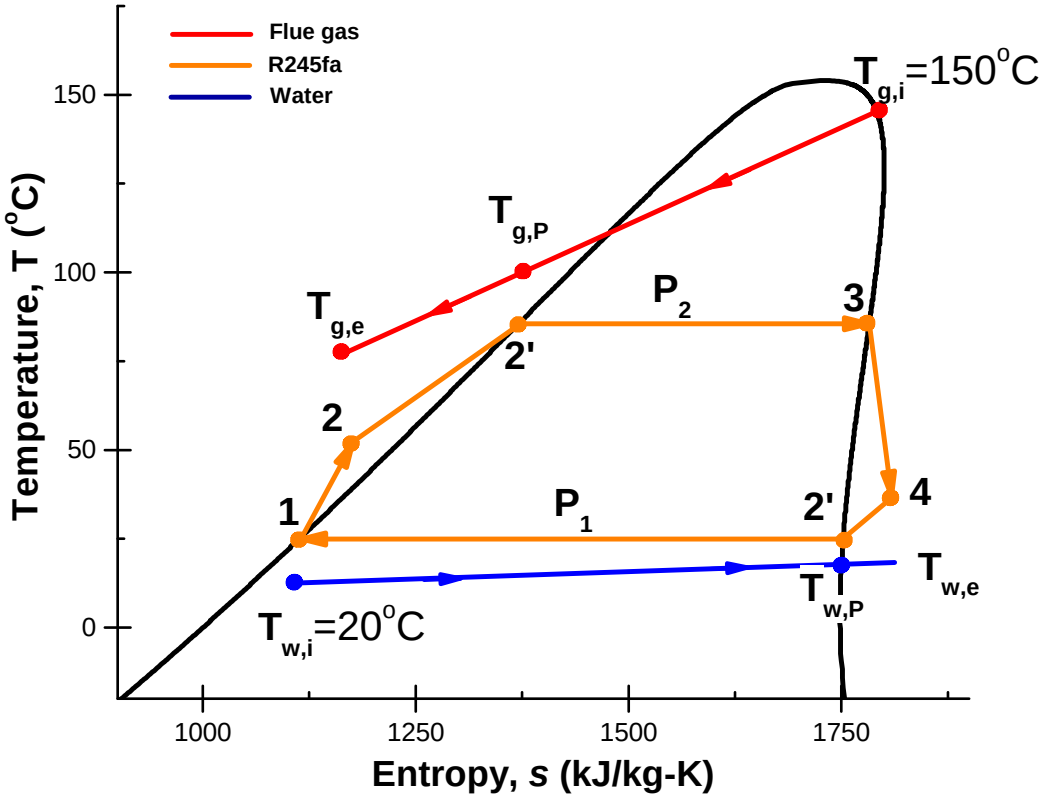


Figure 2.1: An ORC performed in the $T$-$s$ phase diagram of R245fa with coal-fired power plant flue gas as a hot source.

### 2.2.2 Assumptions

To make the problem mathematically tractable our analysis assumed (1) steady state operation and (2) negligible kinetic and potential energy changes for all components, and (3) pressure drop and heat loss in pipes and heat exchangers were negligible. (4) The availability of cooling water was assumed to be large enough such that it could completely cool the working fluid. (5) The hot flue gas was approximated using real properties of air because of the similar composition of flue gas and air (Table 1.2). (6) In the analysis of the ORC and TRC, we assumed that saturated liquid entered the pump. (7) In the analysis of the ORC we assumed saturated vapor entered the turbine (see Figure 2.1 and Figure 2.2). (8) It was also assumed that the heat exchanger surface areas were sufficient to transfer the heat required.

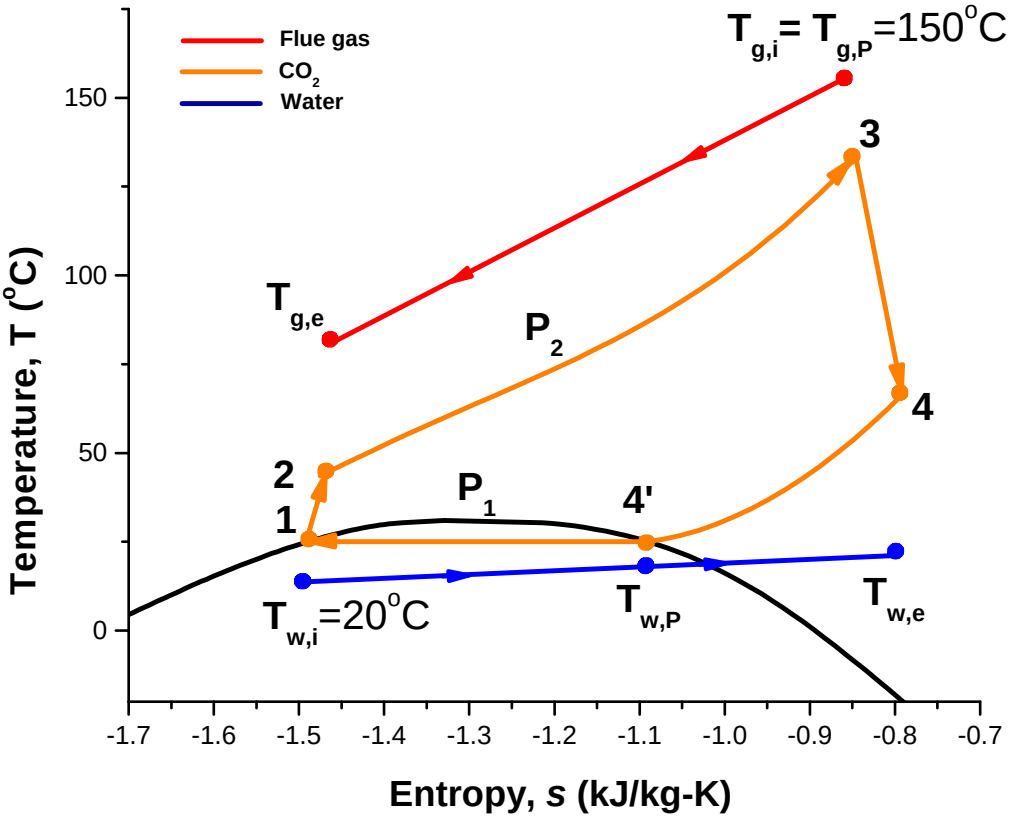


Figure 2.2: A TRC performed in the $T$-$s$ phase diagram of $CO_2$ with coal-fired power plant flue gas as a hot source.

(9) Moreover, it was assumed that the ORC and TRC were performing heat recovery from the flue gas from the stack of a 500 MW coal-fired power, a typical size [9].

By definition, the pinch point temperature difference refers to the minimum temperature difference for a fluid in a heat exchanger [61]. For both the ORC and TRC, the pinch point between the cold source and the working fluid was assumed to occur when the working fluid was at the saturated vapor state, or between $T_{w,P}$ and $T_{2'}$. For the ORC, the pinch point between the hot source and the working fluid was assumed to occur when the working fluid was at the saturated liquid state, or between $T_{g,P}$ and $T_{2'}$. In the TRC, the location of the pinch point temperature difference was located at the inlet to the turbine rather than at the beginning of phase change (see Figure 1.7). Therefore, $T_{g,P}$ becomes $T_{g,i}$ and $T_{2,P}$

becomes $T_3$. These pinch point temperature difference locations creates constraints where the temperature difference of the working fluid and cold source, or hot source and working fluid at the location of the pinch point temperature difference cannot be less than the pinch point temperature difference $\Delta T$. Mathematically, this can be formulated as,

$$T_{g,P} - T_{2'} \geq \Delta T_g, \tag{2.1}$$

and

$$T_{4'} - T_{w,P} \geq \Delta T_w. \tag{2.2}$$

The pinch point temperature difference in the evaporator $\Delta T_g$ was assumed to be $10^o$C [69–71] and the pinch point temperature difference in the condenser $\Delta T_w$ was assumed to be $3^o$C [69, 72].

### 2.2.3 Governing equations

The processes in each component of the cycle were governed by the first law of thermodynamics. For a control volume with a single inlet and exit under steady-state conditions (assumption 1), the first law of thermodynamics can be written as [56]

$$\dot{Q}_{CV} - \dot{W}_{CV} = \dot{m}\left[\left(h_e + \frac{\nu_e^2}{2} + gz_e\right) - \left(h_i + \frac{\nu_i^2}{2} + gz_i\right)\right], \tag{2.3}$$

where $\dot{Q}_{CV}$ is the net heat transfer to the control volume, $\dot{W}_{CV}$ is the power of the control volume, $\dot{m}$ is mass flow rate of the working fluid, $h$ is the enthalpy, $\nu$ is the average fluid velocity, $g$ is gravitational acceleration, and $z$ is the height for each $k$ fluid in the control volume. Again, the subscripts $i$ and $e$ refer to the inlet and exit, respectively. By convention Equation (2.3) is written such that the heat transfer term is positive for heat entering the control volume and power is positive for power done by the control volume [56].

Neglecting changes in kinetic and potential energies (assumption 2) yields, for all components of the cycle.

$$\dot{Q}_{CV} - \dot{W}_{CV} = \dot{m}\left(h_e - h_i\right), \tag{2.4}$$

Thus, applying Equation 2.4 to the pump, the pump power $\dot{W}_{1\to2}$ can be expressed as

$$\dot{W}_{1\to2} = \dot{m}(h_1 - h_2). \tag{2.5}$$

Here, the pump exit enthalpy $h_2$ was calculated according to [56],

$$h_2 = \frac{h_{2,s} - h_1}{\eta_{s,pump}} + h_1, \tag{2.6}$$

where $\eta_{s,pump}$ is the isentropic efficiency of the pump and the subscript $s$ refers to the exit enthalpy if the process was isentropically compressed under the same inlet and exit pressures.

Similarly, turbine power $\dot{W}_{3\to4}$ can be expressed as

$$\dot{W}_{3\to4} = \dot{m}(h_3 - h_4), \tag{2.7}$$

where $h_4$ was calculated according to

$$h_4 = \eta_{s,turbine}(h_{4,s} - h_3) + h_3, \tag{2.8}$$

where $\eta_{s,turbine}$ is the isentropic efficiency of the turbine.

Heat transfer from the working fluid to the cooling water in the condenser $\dot{Q}_{2\to3}$ can be expressed as

$$\dot{Q}_{2\to3} = \dot{m}(h_4 - h_1). \tag{2.9}$$

Heat transfer to the working fluid from the hot flue gas in the evaporator $\dot{Q}_{4\to1}$ can be expressed as

$$\dot{Q}_{4\to1} = \dot{m}(h_3 - h_2). \tag{2.10}$$

For both the evaporator and condenser heat transfer was divided into two sections in order to determine the state of the pinch point in the hot source (state g,P), cold source (state w,P), and working fluid (states 2' and 4'). Performing an energy balance between the energy lost by the flue gas and gained by the working fluid in the evaporator (Process 2→3) yields

$$\dot{m}_g(h_{g,i} - h_{g,P}) = \dot{m}(h_3 - h_{2'}), \tag{2.11}$$

and

$$\dot{m}_g(h_{g,P} - h_{g,e}) = \dot{m}(h_{2'} - h_2). \tag{2.12}$$

Similarly, in the condenser (Process 4→1) yields

$$\dot{m}_w(h_{w,e} - h_{w,P}) = \dot{m}(h_4 - h_{4'}), \tag{2.13}$$

and

$$\dot{m}_w(h_{w,P} - h_{w,i}) = \dot{m}(h_{4'} - h_1). \tag{2.14}$$

Table 2.1 summarizes the input parameters used in both the ORC and the TRC thermodynamic models. The flue gas inlet temperature was equal to a common coal-fired power plant flue gas exit temperature, 150$^o$C. The mass flow rate was $\dot{m}_g = 700$ kg/s corresponding to a 500 MW coal-fired power plant, i.e., $T_{g,i} = 150^o$C. The cooling water had an inlet temperature, $T_{w,i} = 20^o$C. Both the flue gas and cooling water were assumed to be at atmospheric pressure, $P_g = P_w$ =101 kPa.

Table 2.1: Input parameters for a R245fa organic Rankine cycle and $CO_2$ transcritical Rankine cycle models with coal-fired power plant flue gas at $T_H = 150^o$C as the hot source.

| | |
|---|---|
| Heat source flow rate, $\dot{m}_g$ | 700 kg/s |
| Heat source inlet temperature, $T_{g,i}$ | 150$^o$C |
| Heat source pressure, $P_g$ | 101 kPa |
| Cooling water inlet temperature, $T_{w,i}$ | 20$^o$C |
| Cold source pressure, $P_w$ | 101 kPa |
| Pump isentropic efficiency, $\eta_{s,pump}$ | 0.8 |
| Turbine isentropic efficiency, $\eta_{s,turbine}$ | 0.8 |
| Temperature of condensation, $T_1$ | 25$^o$C |

The preceding equations resulted in a system 30 equations and 28 property calls for R245fa, $CO_2$, air, and water. With the given input parameters in Table 2.1, these were used to solve for 58 unknowns using the software Engineering Equation Solver (EES) for a given evaporator pressure and working fluid mass flow rate.

### 2.2.4 Performance metrics

Several performance metrics were used to evaluate the ORC and the TRC. The first and most fundamental of these metrics was $\dot{W}_{net}$, the net amount of power produced by the cycle under investigation defined as the sum of the power produced in the turbine $\dot{W}_{3\to4}$ (>0) and

the power required by the pump $\dot{W}_{1\to2}$ (<0),

$$\dot{W}_{net} = \dot{W}_{3\to4} + \dot{W}_{1\to2}. \tag{2.15}$$

The net power does not take into account how efficiently the cycle converts the thermal energy in the hot flue gas heat to useful energy in the form of turbine power. Therefore, two efficiency metrics were introduced. The first was thermal efficiency defined as [56],

$$\eta_{th} = \frac{\dot{W}_{net}}{\dot{Q}_{2\to3}}. \tag{2.16}$$

While thermal efficiency accounts for the magnitude of energy flow, it does not account for the quality of energy flow, a concept quantified by exergy. Exergy flow rate denoted by $\dot{\Psi}_a$, is a value representing the maximum possible useful power of a stream [56]. Exergy flow rates were calculated at all $j$ states for each $a$ component, expressed as [56]

$$\dot{\Psi}_{a,j} = \dot{m}[h_{a,j} - h_0 - T_0(s_{a,j} - s_0)], \tag{2.17}$$

where $s$ is the entropy and the subscript "0" refers to the dead state, taken at $T_0 = 20^o$C and $P_0 = 101$ kPa. Once exergy flow rates were calculated, the rate of irreversibility or exergy destruction rate $\dot{I}_a$ was calculated for each $a$ component according to [56],

$$\dot{I}_a = \dot{\Psi}_{a,i} - \dot{\Psi}_{a,e} - \dot{W}_a. \tag{2.18}$$

Irreversibility represents the value of loss of potential power. At the inlet and exit of the evaporator and condenser the exergy flow rates were summed across two streams: (1) the working fluid and (2) the hot flue gas or cooling water. Moreover, the power term was non-zero for the pump and turbine only.

Next, a so-called second law efficiency $\eta_{II}$ was calculated. Second law efficiency can be thought of as a measure of the thermodynamic matching of a heat source with the system, or alternatively how much potential power is wasted in reference to an inlet fuel source. The second law efficiency for a cycle can be formulated as [69]

$$\eta_{II} = 1 - \frac{\dot{I}_{tot}}{\dot{\Psi}_{g,i}}, \tag{2.19}$$

where $\dot{I}_{tot}$ is the exergy destruction summed across all $n$ components of the cycle, expressed as

$$\dot{I}_{tot} = \sum_{a=1}^{n} \dot{I}_a. \tag{2.20}$$

## 2.3 Results and discussion

### 2.3.1 Preliminary analysis

A simple analysis was first performed in order to provide context for, and validate the subsequent results. As previously mentioned, the maximum efficiency of a power cycle between a cold source at $T_C = 20^o$C and a hot source at $T_H = 150^o$C is equal to the Carnot efficiency of 31%. ICF International [5] reports that commercial ORC systems typically operate at a thermal efficiency of one-third of the maximum efficiency. Thus, between $T_C = 20^o$C and $T_H = 150^o$C, the efficiency of an ORC or TRC is around 10.3%. For a flue gas with constant specific heat $c_p = 1.01$ kJ/kg.K, the input heat transfer rate $\dot{Q}_{in}$ can be defined as

$$\dot{Q}_{in} = \dot{m}_g c_p (T_H - T_C). \tag{2.21}$$

Then, for the mass flow rate $\dot{m}_g = 700$ kg/s corresponding to a 500 MW coal-fired power plant, $\dot{Q}_{in}$ was found to be 92.2 MW. For an ORC with a thermal efficiency of 10.3%, the power generated from the waste heat recovery unit would produce 9.5 MW of electricity.

### 2.3.2 Organic Rankine cycle

In the following results, evaporator pressure $P_2$ and mass flow rate $\dot{m}$ were varied in order to investigate the effects of these variables on the performance of the cycle.

Figure 2.3 shows the net power plotted against the evaporator pressure $P_2$ for the R245fa flow rate $\dot{m}$ of 50 kg/s, 150 kg/s, and 250 kg/s. It indicates that the net power increased with both pressure and mass flow rate but was limited by the pinch point temperature difference in the evaporator [Equation (2.1)]. As the mass flow rate $\dot{m}$ increased, the exit temperature in the hot source decreased. This brought $T_{g,P}$ closer to $T_{2'}$ at a given pressure. This is

graphically illustrated as an increase in the slope of the red flue gas line in Figure 2.1.

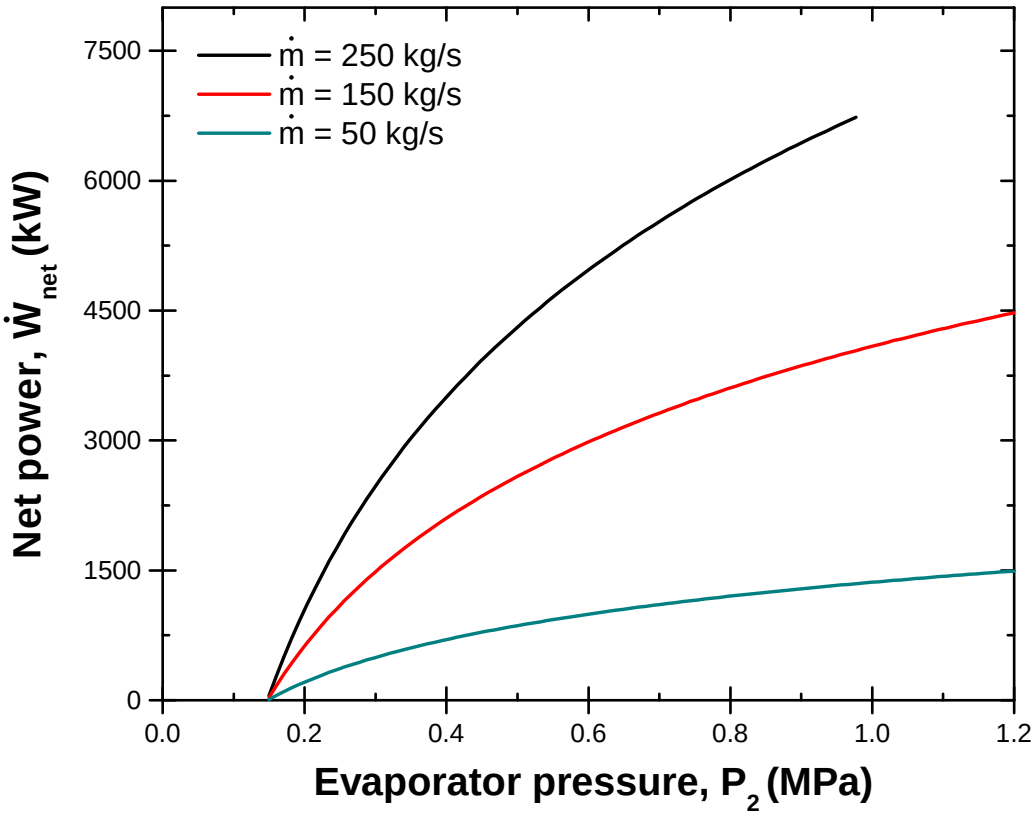


Figure 2.3: Net power $\dot{W}_{net}$ as a function of evaporator pressure $P_2$ for several values of R245fa flow rates $\dot{m}$ for an organic Rankine cycle using hot flue gas at $T_{g,i}$=150$^o$C and $\dot{m}_g$ = 700 kg/s and a cold source at $T_{w,i}$ = 20$^o$C.

Similarly, an increase in evaporator pressure brought $T_{g,P}$ closer to $T_{2'}$. As evaporate pressure increased, so did the temperature of R245fa in the evaporator. Moreover, as the cycle operated between larger pressure differences, $P_1$ and $P_2$, the working fluid was able to expand more in the turbine. Note that for the flow rate $\dot{m}$ = 250 kg/s, the values of evaporator pressure considered broke the pinch point temperature constraint [Equation (2.1)].

Figure 2.4 plots the thermal efficiency $\eta_{th}$ of the ORC as a function of the evaporator pressure $P_2$. It indicates that the thermal efficiency $\eta_{th}$ increased at a decreasing rate with increasing evaporate pressure $P_2$. This can be attributed to two reasons: (1) for a given evaporator pressure $P_2$ all states of the working fluid are fixed and (2) both net power and

heat transfer in the evaporator are linearly proportional to the working fluid mass flow rate $\dot{m}$.

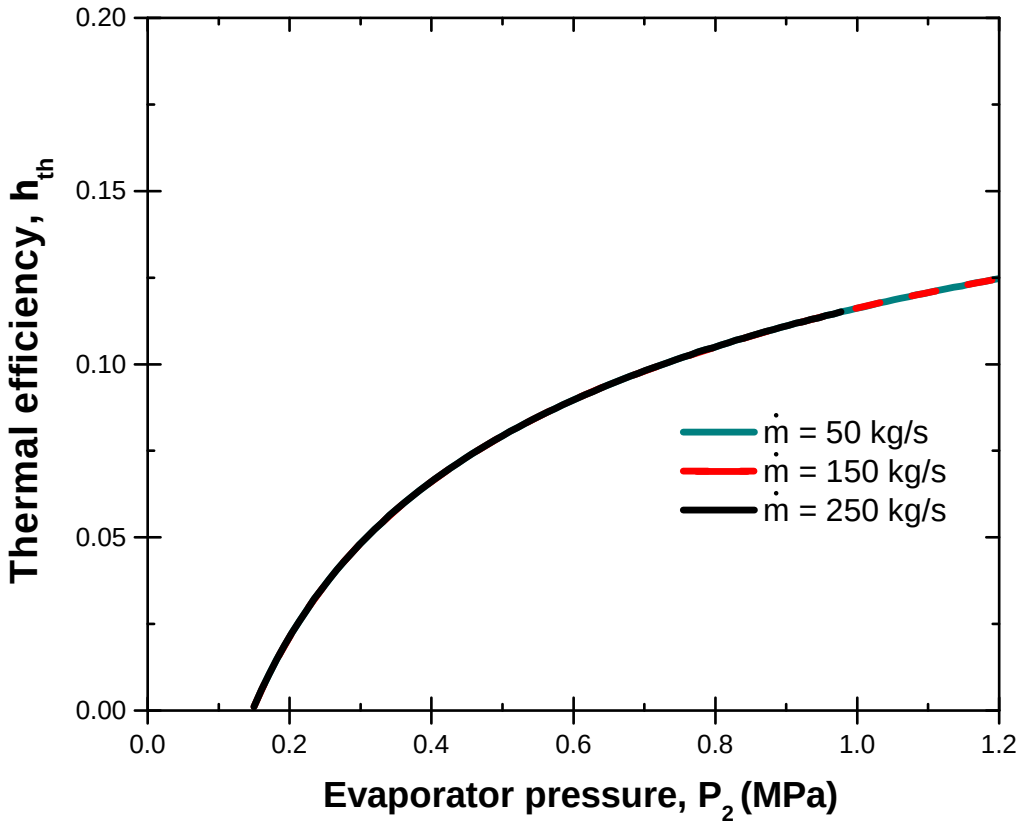


Figure 2.4: Thermal efficiency $\eta_{th}$ as a function of evaporator pressure $P_2$ for several values of R245fa flow rates $\dot{m}$ for an organic Rankine cycle using hot flue gas at $T_{g,i} = 150^o$C and $\dot{m}_g = 700$ kg/s and a cold source at $T_{w,i} = 20^o$C.

As mass flow rate $\dot{m}$ decreased, higher evaporator pressures could be achieved without breaking the pinch point constraint. Thus, the thermal efficiency $\eta_{th}$ was maximum for an infinitesimally small mass flow rate $\dot{m}$, as it allows the evaporator pressure to increase without lowering the pinch point of the flue gas and R245fa in the evaporator. Therefore, it is not sensible to operate the cycle optimized for maximum thermal efficiency.

In order to evaluate the second law efficiency $\eta_{II}$ [Equation 2.19], irreversibility $\dot{I}_a$ was calculated for each component of the ORC cycle (i.e, the pump, turbine, condenser, and evaporator). Figures 2.5.a and 2.5.b plot $\dot{I}_a$ for $\dot{m}$=50 kg/s and $\dot{m}$ = 250 kg/s flow rates, respectively. They indicate that the pump contributed the least irreversibility among all

components. Irreversibility of the pump and turbine increased with evaporator pressure $P_2$ because there was a larger change in enthalpy at higher pressure. However, irreversibility in the turbine increased at a faster rate. This was due to the fact that the vapor phase experienced larger enthalpy changes as the result of changes in pressure. By contrast, the condenser irreversibility was constant with evaporator pressure.

Irreversibility in the evaporator contributed the most to the total irreversibility. This irreversibility decreased with increasing evaporator pressures. As mentioned earlier, higher evaporator pressure caused higher temperature for the working fluid. This resulted in a smaller temperature difference between the hot flue gas and the R245fa working fluid. A smaller temperature difference introduces less entropy generation, and thus less irreversibility.

Figure 2.6 plots the influence of evaporator pressure on second law efficiency $\eta_{II}$ for flow rates $\dot{m} = 50$ kg/s and $\dot{m} = 250$ kg/s. It indicates that higher flow rates $\dot{m}$ resulted in lower second law efficiency. Referring to Equation (2.19), because $\dot{\Psi}_{g,i}$ was constant, second law efficiency was determined by the magnitude of total irreversibility $\dot{I}_{tot}$ which was a function of working fluid mass flow rate. For a given flow rate, as the evaporator pressure increased, the second law efficiency increased with diminishing returns. As described earlier this was because higher evaporator pressure led to higher evaporator temperature which resulted in a lower temperature difference and thus lower entropy generation in the evaporator.

### 2.3.3 Transcritical Rankine cycle

Figure 2.7 plots the net power $\dot{W}_{net}$ as a function of the evaporator pressure $P_2$ for the $CO_2$ flow rate $\dot{m}$ of 50 kg/s, 150 kg/s, and 250 kg/s. Similar to the ORC, Figure 2.7 indicates that a positive relationship existed between the net power $\dot{W}_{net}$ and the mass flow rate $\dot{m}$ for a given evaporator pressure. All mass flow rates followed the same relationship with evaporator pressure, namely increasing at diminishing rates, hitting a peak, and then declining. For the mass flow rates considered this peak occurred at 16 MPa. Unlike the ORC, the TRC reached peak power before the pinch point constraint [Equation (2.1)] set in.

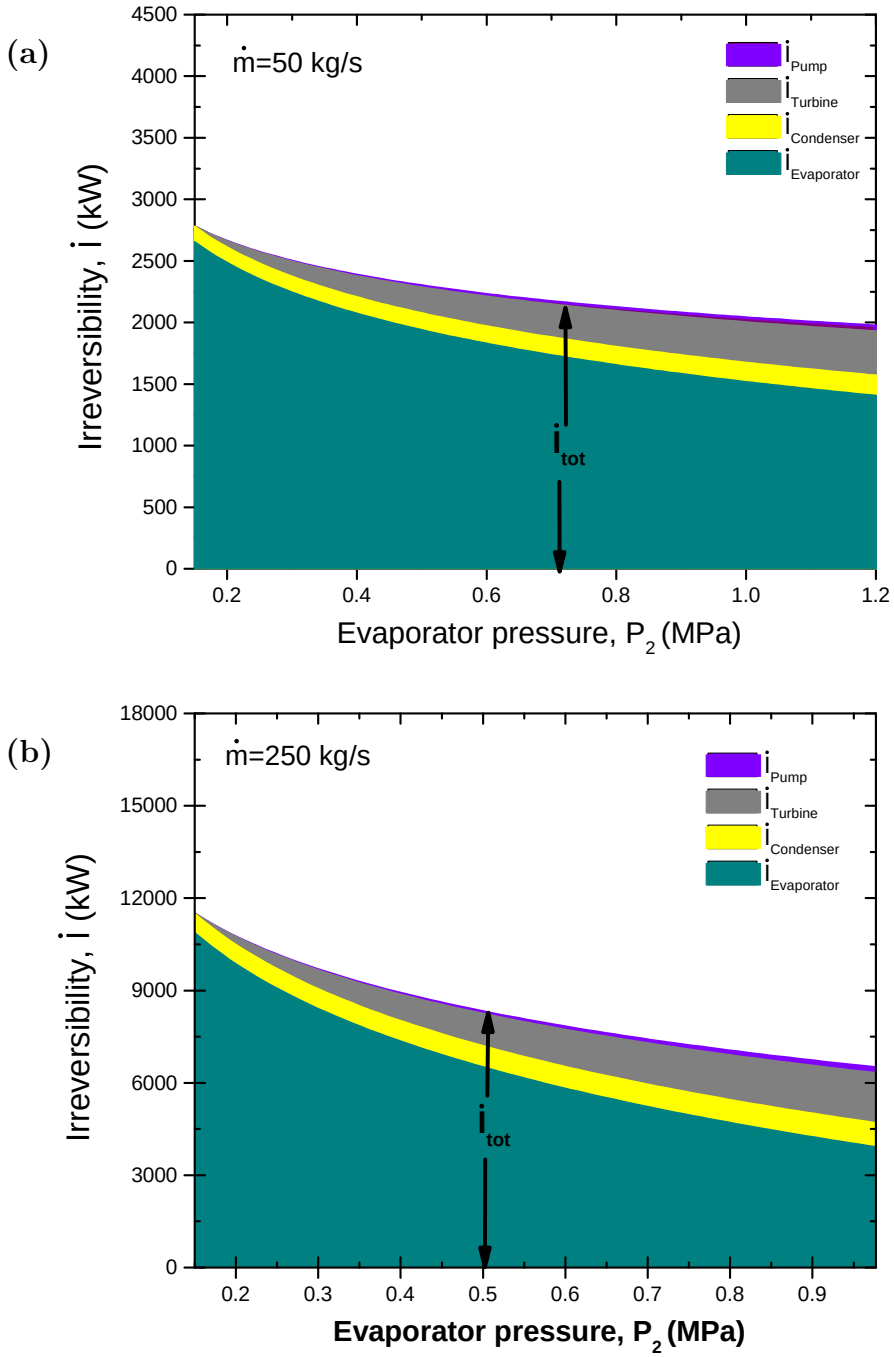


Figure 2.5: Irreversibility $\dot{I}$ as a function of evaporator pressure $P_2$ for R245fa values of mass flow rate $\dot{m}$ of (a) 50 and (b) 250 kg/s for all components for an organic Rankine cycle using hot flue gas at $T_{g,i} = 150^{o}$C and $\dot{m}_g = 700$ kg/s and a cold source at $T_{w,i} = 20^{o}$C.

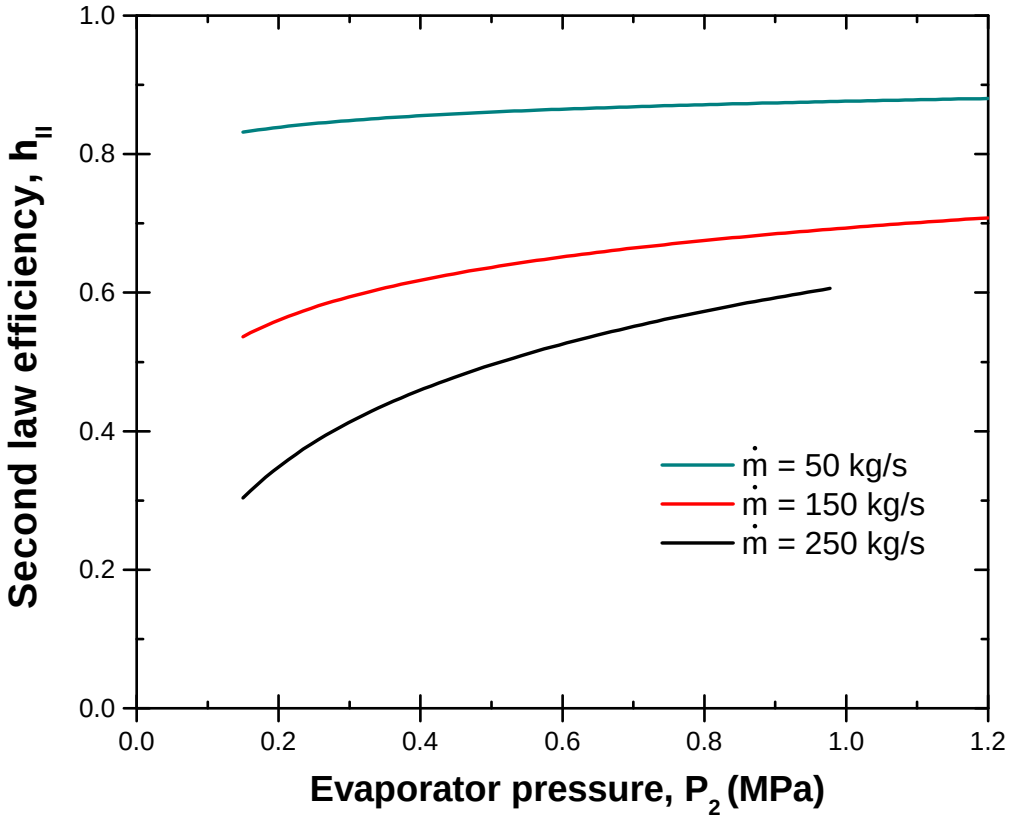


Figure 2.6: Second law efficiency $\eta_{II}$ as a function of evaporator pressure, $P_2$, for several values of R245fa flow rates $\dot{m}$ for an organic Rankine cycle using hot flue gas at $T_{g,i} = 150^o$C and $\dot{m}_g = 700$ kg/s and a cold source at $T_{w,i} = 20^o$C.

Figure 2.8 plots the thermal efficiency $\eta_{th}$ as a function of the evaporator pressure $P_2$. Similar to the ORC, thermal efficiency was constant between flow rates and increased at a decreasing rate.

Figure 2.9 plots the irreversibility $\dot{I}_a$ as a function of the evaporator pressure $P_2$ for the mass flow rates $\dot{m} = 50$ kg/s and $\dot{m} = 250$ kg/s. Irreversibility in the evaporator decreased with evaporator pressure for the same reason as the ORC, namely that the average temperature difference between the working fluid and hot source was lower as evaporator pressure increased. Unlike the ORC, irreversibility in the condenser also decreased as evaporator pressure increased. This is due to how the models were defined. In the ORC, the heating in the evaporator stopped when the fluid became a saturated vapor. In the TRC, the heating in the evaporator ended when the fluid reached the pinch point. In other words, the ORC heating

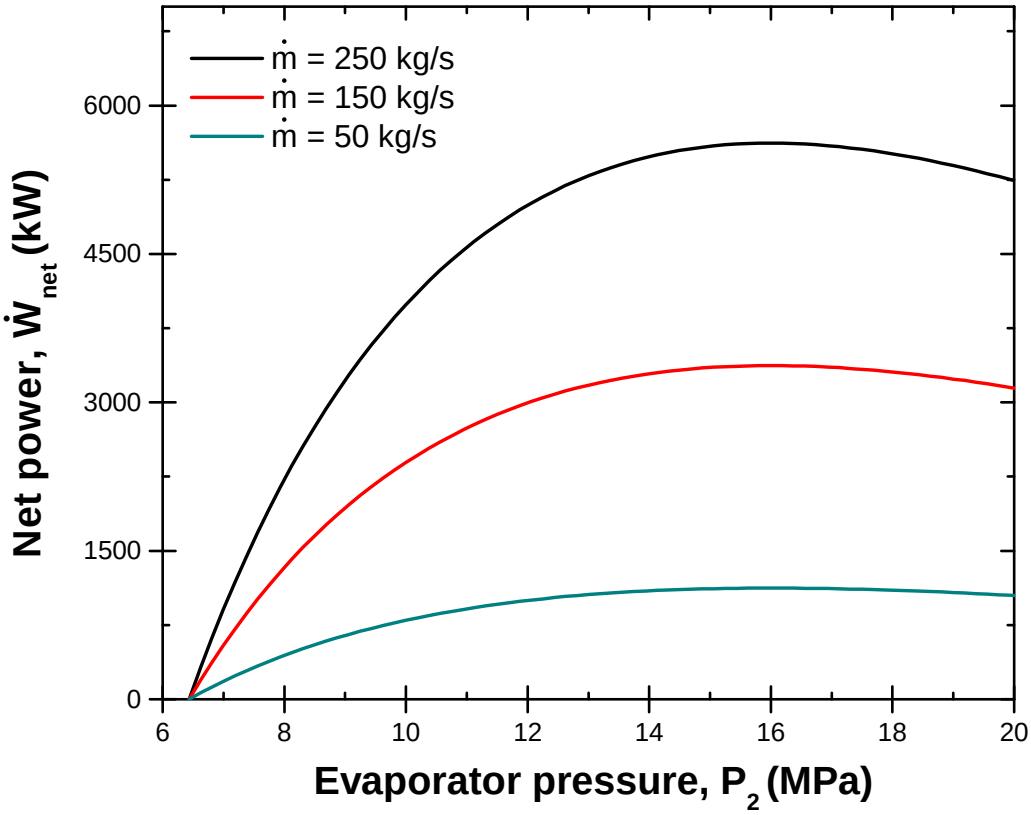


Figure 2.7: Net power $\dot{W}_{net}$ as a function of evaporator pressure $P_2$ for several values of flow rates $\dot{m}$ for a transcritical Rankine cycle using hot flue gas at $T_{g,i} = 150^o$C and $\dot{m}_g = 700$ kg/s and a cold source at $T_{w,i} = 20^o$C.

was constrained by the dome of saturation while the TRC was constrained by the temperature difference between the working fluid and flue gas. Therefore, the amount of heating $\dot{Q}_{2\to3}$, and therefore cooling $\dot{Q}_{4\to1}$, was relatively constant among evaporator pressures for the ORC, but not for the TRC.

Figure 2.10 plots the second law efficiency $\eta_{II}$ against the evaporator pressure $P_2$ for the TRC. Second law efficiency appeared to follow same trend as the ORC in Figure 2.6.

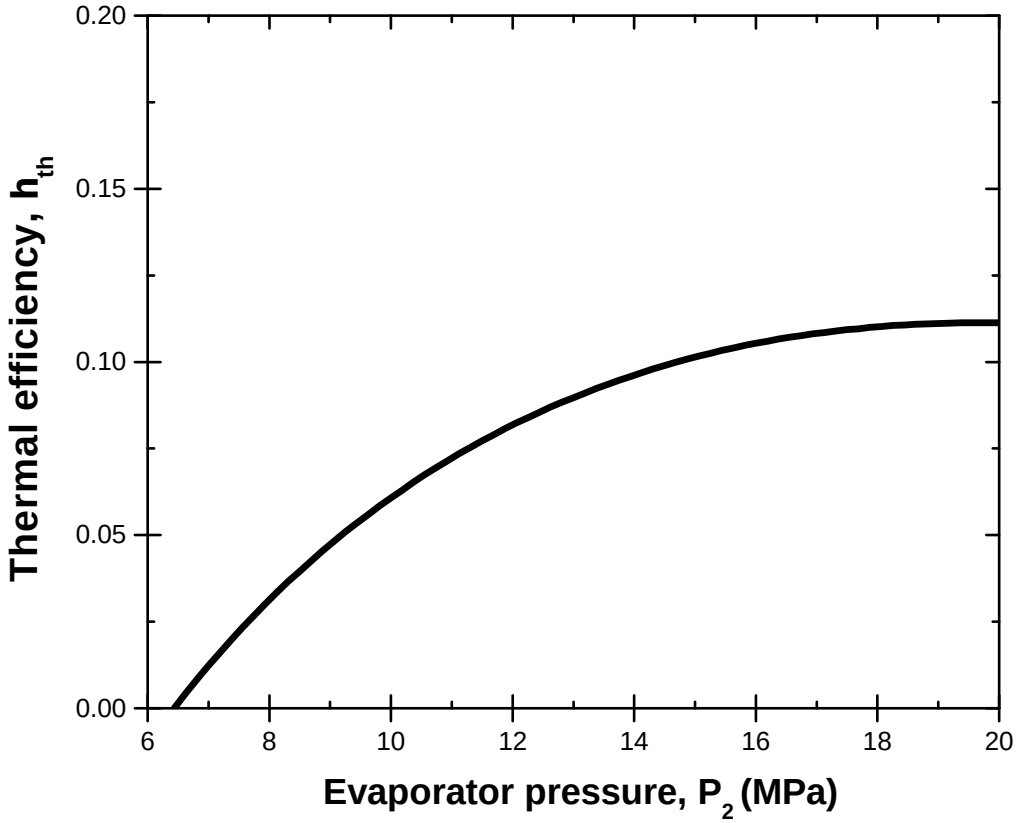


Figure 2.8: Thermal efficiency $\eta_{th}$ as a function of evaporator pressure $P_2$ for a transcritical Rankine cycle using hot flue gas at $T_{g,i} = 150^o$C and $\dot{m}_g = 700$ kg/s and a cold source at $T_{w,i} = 20^o$C.

### 2.3.4 Discussion

In order to compare the performance of the ORC and TRC cycles operating at various levels of evaporator pressure $P_2$, the thermodynamic mean temperature $T_{avg}$ is defined as [73]

$$T_{avg} = \frac{h_2 - h_1}{s_2 - s_1}. \tag{2.22}$$

Additionally, for the purpose of comparison mass flow rates $\dot{m}$ at each thermodynamic mean temperature $T_{avg}$ were chosen such that net power was maximized.

Figure 2.11 plots (a) the net power $\dot{W}_{net}$ and (b) the thermal efficiency $\eta_{th}$ for the ORC using R245fa and the TRC using $CO_2$ as functions of thermodynamic mean temperature $T_{avg}$ in the evaporator with hot flue gas as the hot source at $T_{g,i} = 150^o$C and $\dot{m}_g = 700$ kg/s from a 500 MW power plant and a cooling water source at $T_{w,i} = 20^o$C.. The mass flow rate

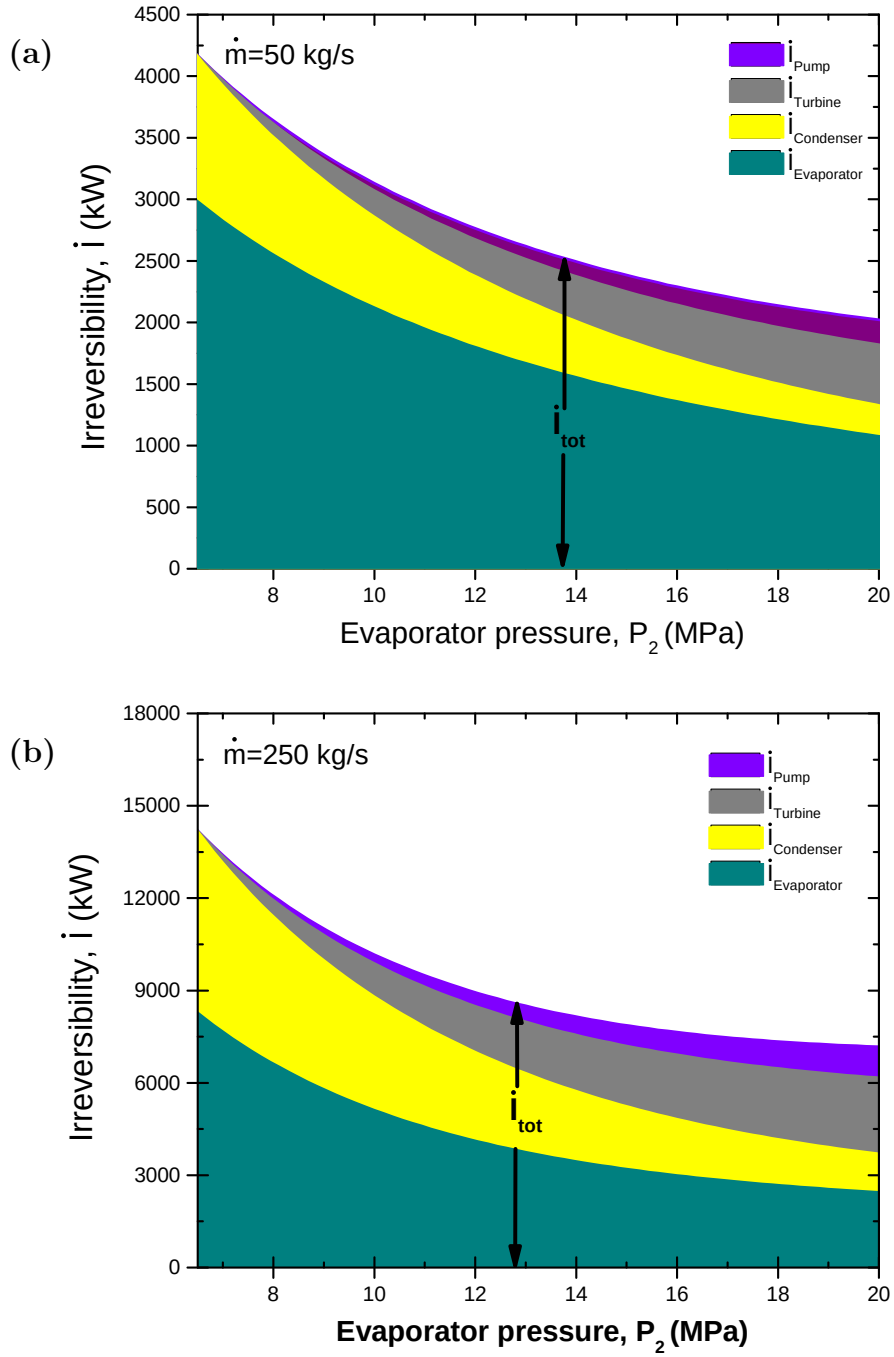


Figure 2.9: Irreversibility $\dot{I}$ as a function of the evaporator pressure $P_2$ for values of $CO_2$ mass flow rate $\dot{m}$ of (a) 50 and (b) 250 kg/s for all components for a $CO_2$ transcritical Rankine cycle using hot flue gas at $T_{g,i} = 150^oC$ and $\dot{m}_g = 700$ kg/s and a cold source at $T_{w,i} = 20^oC$.

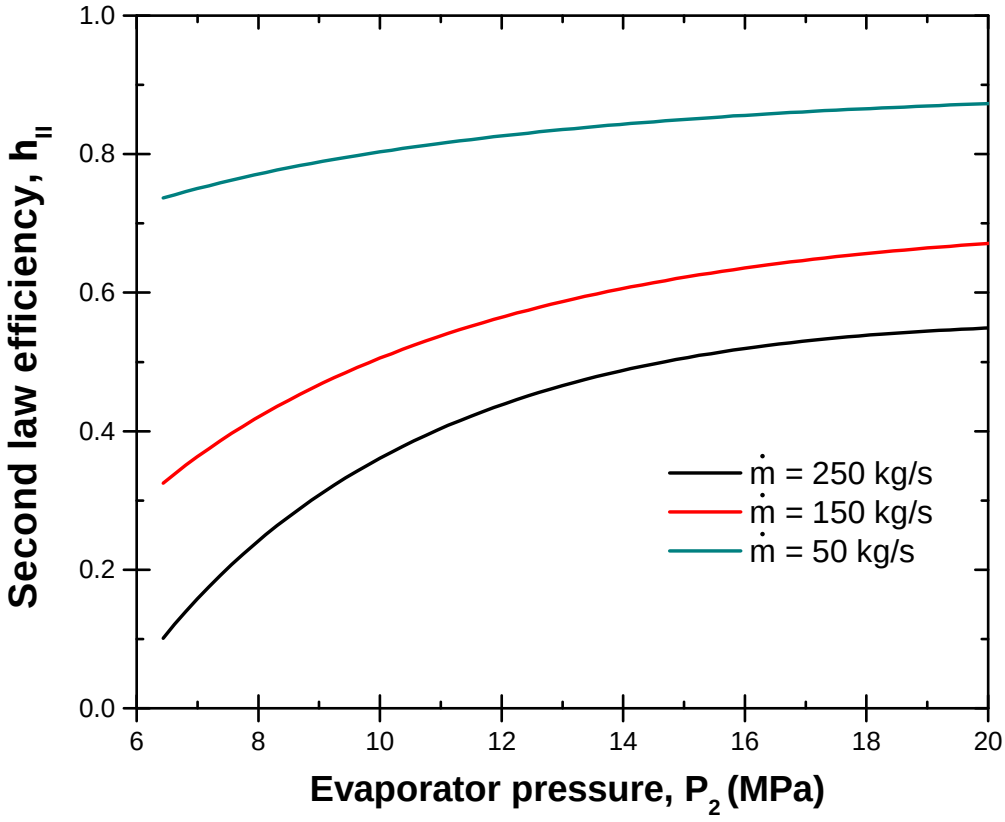


Figure 2.10: Second law efficiency $\eta_{II}$ as a function of the evaporator pressure $P_2$ for several $CO_2$ flow rates $\dot{m}$ for a transcritical Rankine cycle using hot flue gas at $T_{g,i} = 150^oC$ and $\dot{m}_g$ = 700 kg/s and a cold source at $T_{w,i} = 20^oC$.

$\dot{m}$ was optimized at each $T_{avg}$ to maximize the net power $\dot{W}_{net}$.

Net power for both fluids followed approximately the same behavior. However, for a given thermodynamic mean temperature $T_{avg}$ the TRC produced more net power. In fact, the ORC and TRC produced a maximum net power of 6850 kW and 7850 kW, respectively. Interestingly, both cycles achieved maximum net power at $T_{avg} = 76^oC$. Additionally, the ORC achieved maximum power at the flow rate $\dot{m}$ = 256 kg/s and the evaporator pressure $P_2$ = 0.9 MPa. On the other hand, the TRC achieved maximum power at the flow rate $\dot{m}$ = 284 kg/s and the evaporator pressure $P_2$ = 14.4 MPa. At the maximum power the ORC and TRC cycles had thermal efficiencies of 13.0% and 11.4%, respectively.

Moreover, the thermal efficiency of the two cycles were approximately equivalent for low values of $T_{avg}$ ($\leq 65^oC$). However, the thermal efficiency of the TRC decreased for $T_{avg}$ beyond

$85^o$C while the thermal efficiency of the ORC continued to increase linearly with $T_{avg}$. Table 2.3 summarizes the parameters of the ORC and the TRC that resulted in the maximum net power $\dot{W}_{net}$.

In the preliminary analysis presented in Section 2.3.1, the thermal efficiency of the ORC was estimated to be 10.3% for a maximum power of 9500 kW (or 1/3 of the Carnot efficiency). On the other hand, the estimated maximum power was high than that obtained with our thermodynamic models. Table 2.3 summarizes the differences between the values estimated in the preliminary analysis and those calculated by the thermodynamic models for both the ORC with R245fa and TRC with $CO_2$.

Finally, note that cycle modifications such as regeneration and reheating which can increase cycle performance were excluded from the model. In addition, superheating of R245fa in the ORC was not considered. Therefore, while the preliminary analysis overestimated net power, this gap might close as these processes are considered.

Cycle modifications should be studied before concluding whether an organic Rankine cycle using R245fa or a transcritical Rankine cycle fluid using $CO_2$ would produce more net power. Also, the study should be extended to other fluids. Additional factors should also be considered when comparing these power cycles for actual operation. First, $CO_2$ has a relatively high density, and considering that mass flow rates between cycles were similar, the TRC will likely be more compact than the ORC [16]. This is important because smaller equipment can lead to lower capital costs [74]. On the other hand, pressure also plays a large factor in determining the price of process equipment [75]. Therefore, because the $CO_2$ transcritical Rankine cycle operates with very high evaporator pressures, the pump and turbine costs will likely be higher than those for the ORC. Finally, working with high pressure equipment introduces additional hazard in cycle operation [76].

## 2.4 Conclusion

An organic Rankine cycle with R245fa as the working fluid and a transcritical Rankine cycle with $CO_2$ as the working fluid were considered for the purpose of waste heat recovery

Table 2.2: Summary of the parameters that result in the maximum net power for (i) an organic Rankine cycle and (ii) transcritical Rankine cycle for waste heat recovery from a 500 MW coal-fired power plant.

| | | **Cycle parameters** | | | **Optimum design values** | |
|---|---|---|---|---|---|---|
| | Working fluid | Flue gas temperature, $T_{g,i}$ | Hot source flow rate, $\dot{m}_g$ | Cold source temperature, $T_{w,i}$ | Working fluid mass flow rate, $\dot{m}$ | Evaporator pressure, $P_2$ |
| Organic Rankine cycle | R245fa | 150$^o$C | 700 kg/s | 20$^o$C | 256 kg/s | 0.9 MPa |
| Transcritical Rankine cycle | $CO_2$ | 150$^o$C | 700 kg/s | 20$^o$C | 284 kg/s | 14.4 MPa |



Table 2.3: Comparison of net power $\dot{W}_{net}$ and thermal efficiency $\eta_{th}$ between the estimated and modeled values for (i) an organic Rankine cycle performed on R245fa and (ii) a transcritical Rankine cycle performed on $CO_2$ using hot flue gas at $T_{g,i} = 150^o$C and $\dot{m}_g = 700$ kg/s from a 500 MW power plant.

| | **Net power,** $\dot{W}_{net}$ | | | **Thermal efficiency,** $\eta_{th}$ | | |
|---|---|---|---|---|---|---|
| | Estimate | Model | % difference | Estimate | Model | % difference |
| Organic Rankine cycle | 6850 kW | 9500 kW | -27.9% | 13.0% | 10.3% | 26.2% |
| Transcritical Rankine cycle | 7850 kW | 9500 kW | -17.4% | 11.4% | 10.3% | 10.7% |

from the flue gas of a 500 MW coal-fired power plant exiting the stack at $T_H = 150^oC$ and flow rate of $\dot{m}_g = 700$ kg/s. The cold source was taken at $T_C = 20\ ^oC$. At operating conditions maximized for net power ($\dot{m} = 256$ kg/s and $P_2 = 0.9$ MPa), the ORC was found to generate 6850 kW of electricity at 13.0% thermal efficiency. Similarly, at operating conditions maximized for net power ($\dot{m} = 284$ kg/s and $P_2 = 14.4$ MPa), the TRC was found to generate 7850 kW of net power at 11.4% thermal efficiency. Similar analysis should be extended to other working fluids and should consider various Rankine cycle modifications before determining the optimal cycle for waste heat recovery of flue gas.

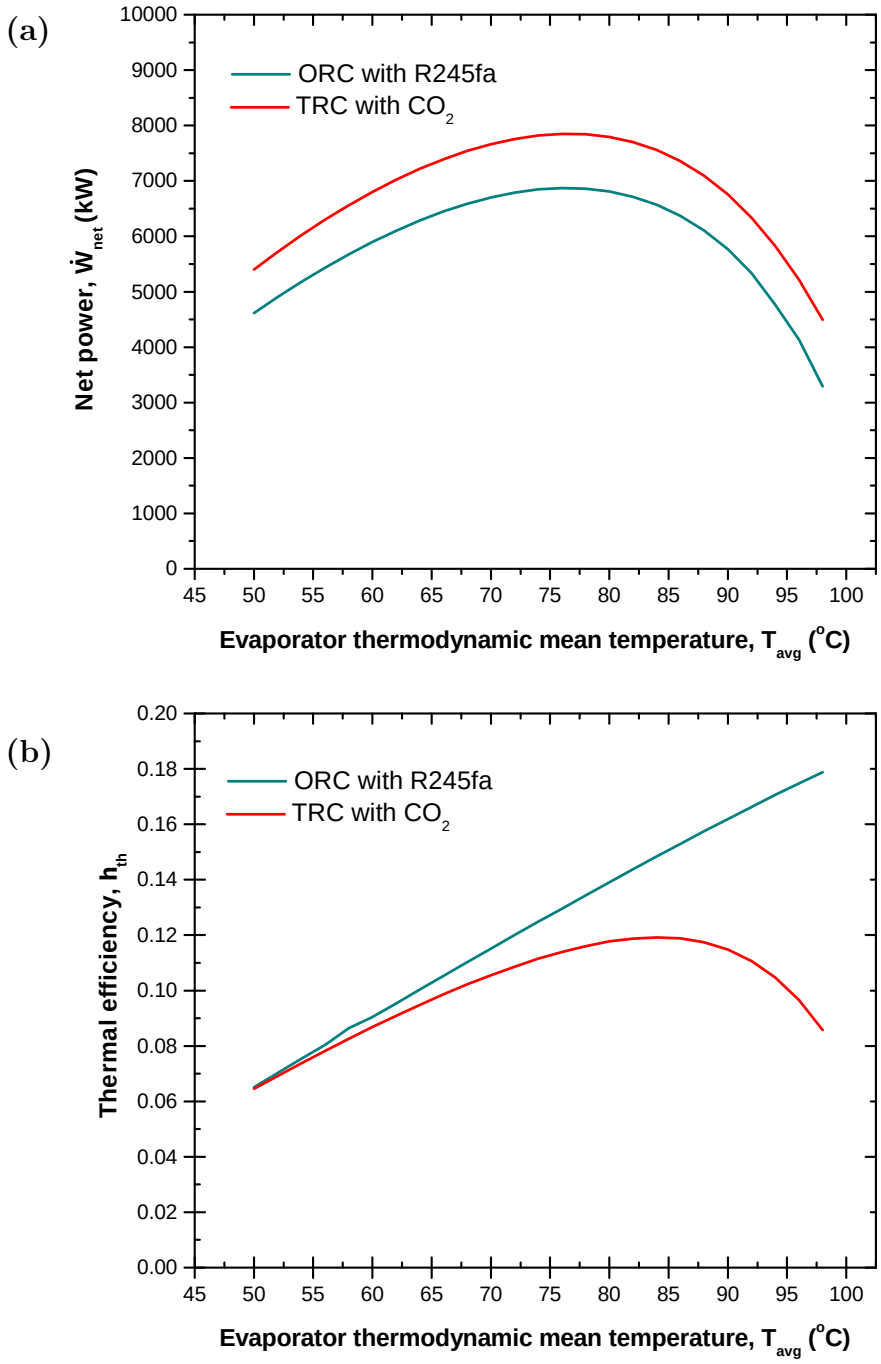


Figure 2.11: (a) Net power $\dot{W}_{net}$ and (b) thermal efficiency $\eta_{th}$ as functions of the thermodynamic mean temperature $T_{avg}$ with flow rate $\dot{m}$ optimized to maximize the net power $\dot{W}_{net}$ for an (i) an organic Rankine cycle performed on R245fa and (ii) a transcritical Rankine cycle performed on $CO_2$ using hot flue gas at $T_{g,i} = 150^oC$ and $\dot{m}_g = 700$ kg/s from a 500 MW coal-fired power plant.

# CHAPTER 3

# Compressed carbonation in the $CO_2$NCRETE production process

## 3.1 Introduction

In the last step of the $CO_2$NCRETE production process described in Section 1.2, 3D printed portlandite reacts with compressed $CO_2$. For this carbonation process, the fraction of the portlandite that undergoes carbonation increases with increasing $CO_2$ pressure [77]. Note that the carbonation reaction rate and the maximum percentage of portlandite carbonated are not determined by the total pressure of the flue gas, but by the $CO_2$ partial pressure [21, 77]. As a result, enrichment can be used to increase the $CO_2$ concentration of the gas mixture and thus increase the $CO_2$ partial pressure without increasing the pressure of the mixture. Additionally, in order to produce large amounts of $CO_2$NCRETE for a given level of flue gas input, the pressurized carbonation can be performed in two stages. The first stage of portlandite carbonation is performed with a stream of coal-fired power plant flue gas while the second stage occurs with a stream of $CO_2$ enriched gas.

## 3.2 Analysis

### 3.2.1 Schematic and description

Figure 3.1 shows a flow diagram of the compressed carbonation processes for $CO_2$NCRETE production with labeled sections. Coal-fired power plant flue gas at point A at $T_A = 25^oC$ enters the system with a pressure of $P_A = 101$ kPa. This mixture is split into two streams;

(1) the stream at point B is the gas that is sent to the un-enriched, or first, carbonation stage and the stream at point C is gas that is ultimately sent to the enriched, or second, carbonation stage. From point B to point F the flue gas is combined with the mixture at point J which consists of excess gas from the second carbonation stage. This mixture is then compressed to point F. At point F the mixture undergoes the carbonation process and then is exhausted as a waste stream at point G.

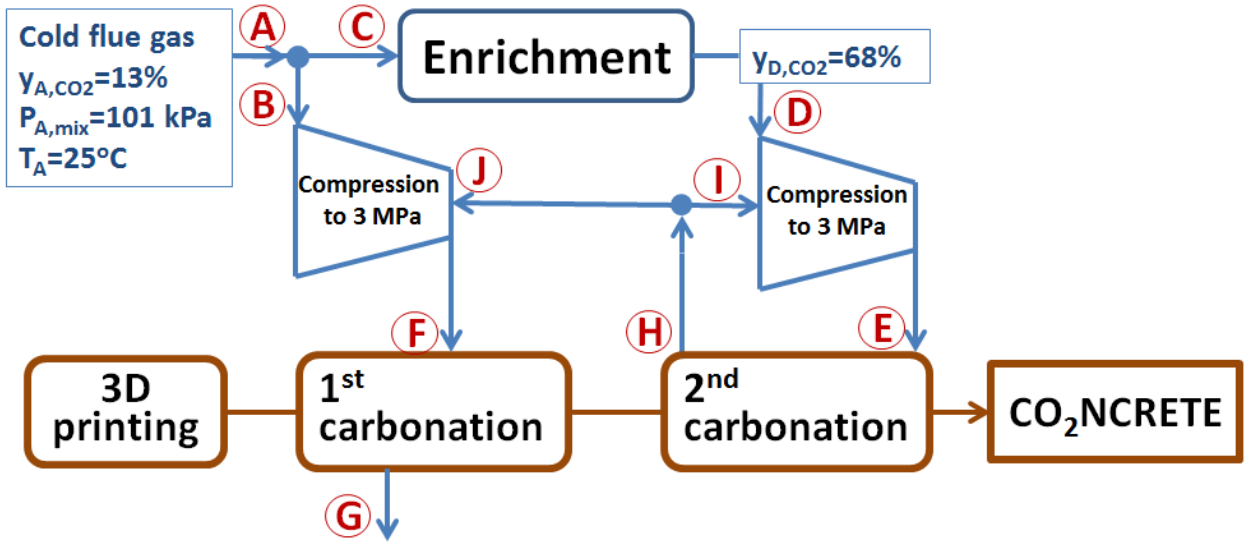


Figure 3.1: A flow diagram of the two-stage compression and carbonation processes for a low carbon footprint building material, $CO_2$NCRETE, production.

The enriched stream is filtered through the membrane from point C to D. From point B to point F the flue gas is combined with the mixture at point I which is reused gas from the second carbonation stage. The mixture is then compressed to point E. From point E to H the enriched mixture undergoes the carbonation reaction. Because the flue gas still has a relatively high $CO_2$ content it is reused with portions going to point J and point I rather than being exhausted. After the second carbonation reaction, the $CO_2$NCRETE production process is complete. Additionally, in order to fill and empty the reaction chamber, the production of $CO_2$NCRETE is made in discrete batches.

### 3.2.2 Ideal gas analysis

Two key ideal gas relations were used in this analysis. First, the mole fraction of gas "$j$" in the flue gas $y_j$, was determined by Amagat's law expressed as [56]

$$y_j = \frac{V_j}{V_{mix}}, \tag{3.1}$$

where $V_j$ is the volume of constituent $j$ and the total volume of the gas mixture is denoted by $V_{mix}$. Second, the partial pressure of the gas $P_j$ was determined by Dalton's law, expressed as [56]

$$P_j = y_j P_{mix}. \tag{3.2}$$

Next, the coal-fired power plant flue gas composition was found. Table 1.2, presented in Section 1.1.1, summarized the composition of flue gas exiting the stack at 150$^o$C and 101 kPa. It showed that 6.20% of coal-fired power plant flue gas was water by volume. The $CO_2$NCRETE production process, however, uses cold flue gas at ambient temperature, taken as 25$^o$C. The mixture composition presented in Table 1.2 cannot sustain this amount of water vapor at the ambient temperature. In fact, at ambient temperature the water condenses out of the mixture until its partial pressure decreases to the saturated pressure. At 25$^o$C the pressure of condensation of water $P_{cond}$ is 3.17 kPa. The partial pressure of water in a gas at 101 kPa and a molar content of 6.20% is 6.26 kPa. Therefore, water condenses out of the mixture until the partial pressure of the water reaches 3.17 kPa. Using Dalton's law [Equation (3.2)] this can be expressed algebraically as,

$$P_{cond} = \frac{n_{H2O}}{n_{O2} + n_{CO2} + n_{O2} + n_{N2} + n_{H2O}}, \tag{3.3}$$

where $n_j$ is the number of moles of each gas species j in the mixture. Solving for $n_{H2O}$, the water that remains in vapor form was calculated to be 50% of the original amount. In addition, neglecting CO and $NO_x$, the composition of the mixture was recalculated with Equation (3.1). Table 3.1 summarizes the composition of coal-fired plant flue gas after condensation of water vapor to 25$^o$C. The partial pressure and saturation pressure for the other flue gas constituents were such that they did not condense.

Table 3.1: Typical coal-fired power plant flue gas composition after being cooled to 25$^o$C [2].

| **Gas** | (% vol.) |
|---|---|
| $\mathbf{CO_2}$ | 13.12% |
| $\mathbf{H_2O}$ | 3.14% |
| $\mathbf{O_2}$ | 4.58% |
| $\mathbf{N_2}$ | 79.16% |

Moreover, an analysis was performed to determine whether the flue gas mixture could be treated as an ideal gas at 3 MPa. The compressibility factor $Z$ is a measure of how much a real gas deviates from ideal gas behavior and is expressed as

$$Z = \frac{P_{mix} V_{mix}}{n_{mix} RT} \tag{3.4}$$

where $R$ is the ideal gas constant. When the compressibility factor equals unity the gas is ideal and Equations (3.1) to (3.2) are valid. The compressibility factor is a function of the mixture temperature and partial pressure of the gas. Kay's rule is an empirically formulated approximation used to calculate the critical temperature $T_{cr,mix}$ and critical pressure $P_{cr,mix}$ of a mixture. Kay's rule is expressed as [56]

$$T_{cr,mix} = \sum_{j=1}^{n} y_j T_{j,cr} \qquad \text{and} \qquad P_{cr,mix} = \sum_{j=1}^{n} y_j P_{j,crit}. \tag{3.5}$$

where $T_{cr,j}$ and $P_{cr,j}$ are the critical temperature and pressure for gas species "j". In order to evaluate the compressibility factor from the critical temperature and pressure, reduced temperature $T_{R,mix}$ and reduced pressure $P_{R,mix}$ were defined as [56]

$$T_{R,mix} = \frac{T_{mix}}{T_{cr,mix}} \qquad \text{and} \qquad P_{R,mix} = \frac{P_{mix}}{P_{cr,mix}}. \tag{3.6}$$

Using a generalized compressibility chart, the compressibility factor for the flue gas at 3 MPa and 25$^o$C was found to be 0.97. Although the temperature of the gas in the carbonation process is likely to be higher than 25$^o$C, a higher temperature tends to make gases behave more ideally [56]. Therefore, the ideal gas behavior was assumed to hold in the following analysis.

### 3.2.3 Assumptions

To make the problem mathematically tractable, the following assumptions were made: (1) pressure drop was assumed to be negligible in the pipes, (2) the gas mixture was an ideal gas and Amagat's law and Dalton's law were valid, (3) pressure of the gas constituents exiting membrane enrichment was assumed to be equal to the partial pressure of those gas constituents which entered the membrane. (4) Each batch was assumed to operate at steady-state conditions (i.e., no ramp up/down effects). (5) The amount of time for each batch was assumed to be dependent solely on reaction time and the amount of time needed to empty the reaction vessel of building material between batches, assumed to be 1 hour. (6) The pressure limit of the reaction vessel was assumed to be 3 MPa. (7) Additionally, temperature was assumed to be constant and equal to 25$^o$C.

(8) The mole fraction of the 3D printed portlandite sample undergoing carbonation was assumed to be solely a function of reaction time and partial pressure of $CO_2$. This neglected the effects of temperature, geometry, and other elements in the gas mixture. The mole fraction of portlandite carbonated as a function of time reaction time was given by two curves fitted from experimental data at pressures of 0.1 MPa and 1 MPa. At 0.1 MPa, the mole fraction of portlandite converted into $CO_2$NCRETE during the first stage low-pressure carbonation reaction $C_1$ as a function of first stage reaction time $t_1$ was given by [77],

$$C_1 = 0.0622 \ln t_1 + 0.5989. \tag{3.7}$$

At 1 MPa, the mole fraction of portlandite converted into $CO_2$NCRETE during the second stage high-pressure carbonation reaction $C_2$ as a function of second stage reaction time $t_2$ was given by [77],

$$C_2 = 0.0945 \ln t_2 + 0.7558. \tag{3.8}$$

Equations (3.7) to (3.8) were valid for levels of carbonation between 50% and 80% [77].

### 3.2.4 Governing equations

Dalton's law [Equation (3.2)] and the definition of mole fraction was solved for at every point. Additionally, conservation of mass was applied when two streams were combined or split. The total amount of $CO_2$ entering the system $N_{A,CO2}$ was expressed as

$$N_{A,CO2} = \frac{m_{req}}{M_{CO2}}, \tag{3.9}$$

where $M_{CO2}$ is the molar mass of $CO_2$ and $m_{req}$ was a project requirement of the amount of $CO_2$ that must flow through the system in a 24 hour period. This project requirement was 200 kg $CO_2$/day. The amount of $CO_2$ entering per batch $n_{A,CO2}$ was expressed as

$$n_{A,CO2} = \frac{N_{A,CO2}}{t_{tot}}, \tag{3.10}$$

where $t_{tot}$ is the total amount of time for a batch given by

$$t_{tot} = t_1 + t_2 + t_3, \tag{3.11}$$

where $t_1$, $t_2$, and $t_3$ are the times of the first stage carbonation, the second stage carbonation, and the amount of time between batches, respectively.

Mass conservation was performed through the carbonation reaction and given by

$$n_{G,CO2} = n_{F,CO2} - n_{CL}C_1, \tag{3.12}$$

and

$$n_{I,CO2} = n_{E,CO2} - n_{CL}(C_2 - C_1), \tag{3.13}$$

where $n_{G,CO2}$, $n_{F,CO2}$, $n_{I,CO2}$, and $n_{E,CO2}$ are the amount of moles of $CO_2$ in the flue gas at points G, F, I, and E, respectively, while $n_{CL}$ is the amount of carbonated lime product (i.e., $CO_2$NCRETE).

For an ideal gas mixture, enthalpy $\bar{h}_{mix}$ is expressed as [56],

$$\bar{h}_{mix} = \sum_{j=1}^{n} y_j \bar{h}_j, \tag{3.14}$$

and for an ideal gas mixture, entropy $\bar{s}_{mix}$ is given by [56],

$$\bar{s}_{mix} = \sum_{j=1}^{n} y_j \bar{s}_j. \tag{3.15}$$

The work required by the compressor $W_{comp}$ to compress the gas mixture to 3 MPa was expressed as

$$W_{comp} = n_{mix}(\bar{h}_{mix,e} - \bar{h}_{mix,i}), \tag{3.16}$$

where the subscripts $e$ and $i$ refer to the exit and inlet, respectively. The exit enthalpy of the gas mixture $\bar{h}_e$ was expressed as

$$\bar{h}_e = \frac{\bar{h}_{e,s} - \bar{h}_i}{\eta_{s,comp}} + \bar{h}_i, \tag{3.17}$$

where the isentropic efficiency of the compressor $\eta_{isen,comp}$ was assumed to be 0.6.

Table 3.2 summarizes the input parameters used in the model for the two-stage compression production processes of $CO_2$NCRETE.

Table 3.2: Summary of the input parameters used in the model for the two-stage compression production processes of $CO_2$NCRETE.

| | |
|---|---|
| $CO_2$ inlet requirement, $m_{req}$, | 200 kg $CO_2$/day |
| Inlet flue gas $CO_2$ concentration, $y_{A,CO2}$ | 0.1312 |
| Inlet flue gas pressure, $P_A$ | 101 kPa |
| $CO_2$ concentration exiting the membrane, $y_{D,CO2}$ | 0.68 |
| Compressor exit, $P_E$,$P_F$ | 3 MPa |

The preceding formula resulted in a system of 42 equations. The equations consisted of 42 unknowns including the number of moles of flue gas mixture $n_{mix}$, the number of moles of $CO_2$ constituent $n_{CO2}$, the $CO_2$ mole fraction $y_{CO2}$, the total mixture pressure $P_{mix}$, the $CO_2$ partial pressure of the flue gas $P_{CO2}$, the number of moles of $CaCO_3$ at each stage $n_{CL}$, the durationg of the first and second stage carbonation $t$, and the batch time $t_{tot}$. This system of equations was solved using Matlab while compressor work was calculated using properties retrieved in EES.

## 3.3 Results and discussion

### 3.3.1 System points

Table 3.3 summarizes the total mass of flue gas $m_{mix}$, the $CO_2$ mole fraction $y_{CO2}$, and the pressure at each point in the system in order to capture 200 kg $CO_2$/day in the form of the limestone building material. To do so, a coal-fired power plant should provide 2181 kg of flue gas at 0.101 MPa and a $CO_2$ mole fraction of 0.132. As expected, the $CO_2$ mole fraction is constant across the split from points A to points B and C, with 67% of the gas mixture going to the membrane at point C. This system would exhaust 300 kg of flue gas mixture at 0.593 MPa and a $CO_2$ mole fraction of 0.188.

Table 3.3: The mass of the flue gas mixture, the $CO_2$ mole fraction, and the pressure for each point over the period of one day in the two-stage compression system designed for low carbon-footprint building material production (Figure 3.1).

| Point | Mass of mixture per batch, $m_{mix}$ | $CO_2$ mole fraction, $y_{CO2}$ | Mixture pressure, $P_{mix}$ |
|---|---|---|---|
| A | 2181 kg | 0.131 | 0.101 MPa |
| B | 715 kg | 0.131 | 0.101 MPa |
| C | 1466 kg | 0.131 | 0.101 MPa |
| D | 462 kg | 0.680 | 0.041 MPa |
| E | 465 kg | 0.667 | 3.000 MPa |
| F | 1014 kg | 0.253 | 3.000 MPa |
| G | 1089 kg | 0.118 | 0.593 MPa |
| H | 397 kg | 0.618 | 1.132 MPa |
| I | 98 kg | 0.618 | 1.132 MPa |
| J | 300 kg | 0.618 | 1.132 MPa |

### 3.3.2 $CO_2$NCRETE production metrics

Table 3.4 shows the mass of $CO_2$NCRETE produced, the mass of $CO_2$ captured, and the time for each reaction in the $CO_2$NCRETE production process. A total of 472.0 kg of $CO_2$ were captured by the carbonation reaction and 637.6 kg of $CaCO_3$ were produced with a batch time of 3.38 hr. Note that the moles of $CaCO_3$ and $CO_2$ were identical because of stoichiometry in Equation (1.3). Although the mixture spends more time in stage 2 of the carbonation, significantly less carbonation occurs. This is a result of (i) the portlandite being 60% carbonated as it enters stage 2 and (ii) the logarithm relationship between carbonation reaction fraction and time [Equation (3.8)].

Table 3.4: The mass of $CO_2$NCRETE produced, The mass of $CO_2$ captured, and the duration of each compression stage over the period of one day in the two-stage compression system designed for low carbon-footprint building material production.

| Carbonation stage | Mass of $CO_2$NCRETE produced, $m_{HL}$ | Mass of $CO_2$ consumed, $m_{CO2}$ | Duration, $t$ |
|---|---|---|---|
| Stage 1 | 484.7 kg | 358.8 kg | 7.67 hr |
| Stage 2 | 152.9 kg | 113.2 kg | 9.23 hr |
| Total | 637.6 kg | 472.0 kg | 24 hr |

The total amount of work required to power the compressors for a day $W_{comp}$ was 1,014 MJ, or 1,589 kJ/kg of $CO_2$NCRETE. It was divided in 78% for the compression for stage 1 carbonation, and 22% for the compression for stage 2 carbonation.

### 3.3.3 Energy analysis for $CO_2$NCRETE production processes

As discussed in Chapter 2, for a 500 MW coal-fired power plant with flue gas exiting at 150$^o$C at 700 kg/s, the ORC using R245fa and the TRC using $CO_2$ could produce 7850 kW and 6850 kW, respectively. Assuming the process can be scaled to different amounts of flue gas input, 7850 kW generated from 700 kg/s of flue gas is equivalent to 11.2 kW/kg of inlet flue gas. Also, assuming the inlet flue gas is at steady-state conditions, then 11.2 J/kg of inlet

flue gas could be generated from the TRC over a period. If the TRC system were to recover energy from the flue gas entering the two-stage compression system, it would produce 23.6 MJ (taking into account the water that condensed out of the flue gas).

Therefore, if the TRC were to recover energy from the coal-fired power plant flue gas before entering the two-stage carbonation system, it would be able to supply about 2.3% of the 1,589 kJ/kg of $CO_2$NCRETE required. This may not be a useful proportion of energy, especially when considering the capital cost and operating cost of the TRC.

## 3.4 Conclusion

The processes for compressed carbonation in the $CO_2$NCRETE production process were modeled for laboratory scale operation. The mass of the flue gas mixture, the pressure, and the $CO_2$ mole fraction at each stage of the process were evaluated as well as the total energy requirements and the mass of $CO_2$NCRETE produced. It was found that the system would require 1,1014 MJ of work, 2181 kg of flue gas, and produce 637.6 kg of $CO_2$NCRETE per day. When the energy required for compression was compared to the energy that would be recovered from waste heat, it was found that a waste heat harvesting cycle with coal-fired power plant flue gas at 150$^o$C and a cold source at 20$^o$C would produce 2.3% of the required compressor work.

# CHAPTER 4

# Conclusion

This thesis was concerned with making a more efficient $CO_2$NCRETE production process, capturing $CO_2$ into limestone. To this end, thermodynamic models of an organic Rankine cycle with R245fa as the working fluid and a transcritical Rankine cycle with $CO_2$ as the working fluid performing waste heat recovery from a typical 500 MW coal-fired power plant with a flue gas flow rate of $\dot{m} = 700$ kg/s and temperature at $T_H = 150^o$C and cold source at $T_C = 20^o$C were created and evaluated. At operating conditions maximized for net power, the organic Rankine cycle was found to generate 6850 kW of net power with 13.0% thermal efficiency. Similarly, at operating conditions maximized for net power, the transcritical Rankine cycle was found to generate 7850 kW of net power with 11.4% thermal efficiency. However, study of additional fluids and Rankine cycle modifications is needed before choosing the optimal cycle for waste heat recovery. Finally, the two-stage carbonation system in the $CO_2$NCRETE production process was modeled. It was found that the system would require 2,181 kg of flue gas and produce 637.6 kg of $CO_2$NCRETE building material per day. The energy requirement was 1,589 kJ/kg of $CO_2$NCRETE. It was found that the waste heat recovery system could produce 2.3% of the energy required to compress the flue gas at 3 MPa necessary to achieve 79% carbonation in 2.3 hours. If one can tolerate less carbonation and/or longer production time and lower production rate, the pressure can be reduced. Then, the waste heat recovery system will provide an increasing fraction of the energy necessary for compression.

# References


[1] Energy Information Administration, "Annual energy outlook 2014", Tech. Rep. DOE/EIA-0383, U.S. Department of Energy, Washington, D.C., 2014.

[2] X. Xu, C. Song, R. Wincek, J. M. Andresen, B. G. Miller, and A. W. Scaroni, "Separation of $CO_2$ from power plant flue gas using a novel $CO_2$ molecular basket adsorbent", *Division of Fuel Chemistry*, vol. 48, no. 1, pp. 162–163, 2003.

[3] T. Yamamoto, F. Tomohiko, A. Norio, and M. Koichi, "Design and testing of the organic Rankine cycle", *Energy*, vol. 26, no. 3, pp. 239–251, 2001.

[4] Combined Heat and Power Partnership, "Waste heat to power systems", Fact sheet, U.S. Environmental Protection Agency, Washington, D.C., 2012.

[5] A. Elson, R. Tidball, and A. Hampson, "Waste heat to power market assessment", Tech. Rep. TM-2014/620, ICF International, Fairfax, VA, 2015.

[6] EPA, "Inventory of U.S. greenhouse gas emissions and sinks: 1990-2014", Tech. Rep. EPA 430-R-16-002, Environmental Protection Agency, Washington, D.C., 2015.

[7] A. Bland, J. Newcomer, A. Kephart, V. Schmidt, and G. Butcher, "Emissions, monitoring, and control of mercury from subbituminous coal-fired power plants-phase II", Tech. Rep. WRI-08-R012, Western Research Institute, 2008.

[8] M. S. Landis, J. V. Ryan, A. Schure, and D. Laudal, "Behavior of mercury emissions from a commercial coal-fired power plant: The relationship between stack speciation and near-field plume measurements", *Environmental Science & Technology*, vol. 48, no. 22, pp. 13540–13548, 2014.

[9] Energy Information Administration, "Annual electric generator data EIA-860", Database, 2014, "`http://www.eia.gov/electricity/data/eia860/`".

[10] T. Hendricks and W. T. Choate, "Engineering scoping study of thermoelectric generator systems for industrial waste heat recovery", Tech. Rep. (no #), U.S. Department of Energy Industrial Technologies Program, 2006.

[11] B. Saadatfar, R. Fakhrai, and T. Fransson, "Thermodynamic vapor cycles for converting low-to medium-grade heat to power: a state-of-the-art review and future research pathways", *Journal of Macro Trends in Energy and Sustainability*, vol. 2, no. 1, pp. 1–25, 2014.

[12] F. Vélez, F. Chejne, G. Antolin, and A. Quijano, "Theoretical analysis of a transcritical power cycle for power generation from waste energy at low temperature heat source", *Energy Conversion and Management*, vol. 60, pp. 188–195, 2012.

[13] M. Li, J. Wang, S. Li, X. Wang, W. He, and Y. Dai, "Thermo-economic analysis and comparison of a $CO_2$ transcritical power cycle and an organic Rankine cycle", *Geothermics*, vol. 50, pp. 101–111, 2014.

[14] P. Garg, K. Srinivasan, P. Dutta, and P. Kumar, "Comparison of $CO_2$ and steam in transcritical Rankine cycles for concentrated solar power", *Energy Procedia*, vol. 49, pp. 1138–1146, 2014.

[15] V. Dostal, M. J. Driscoll, and P. Hejzlar, "A supercritical carbon dioxide cycle for next generation nuclear reactors", Tech. Rep. MIT-ANP-TR-100, The MIT Center for Advanced Nuclear Energy Systems, Cambridge, MA, 2004.

[16] Y. Chen, P. Lundqvist, and P. Platell, "Theoretical research of carbon dioxide power cycle application in automobile industry to reduce vehicles fuel consumption", *Applied Thermal Engineering*, vol. 25, no. 14, pp. 2041–2053, 2005.

[17] E. Benhelal, G. Zahedi, E. Shamsaei, and A. Bahadori, "Global strategies and potentials to curb $CO_2$ emissions in cement industry", *Journal of Cleaner Production*, vol. 51, pp. 142–161, 2013.

[18] D. N. Huntzinger, J. S. Gierke, S. K. Kawatra, T. C. Eisele, and L. L. Sutter, "Carbon dioxide sequestration in cement kiln dust through mineral carbonation", *Environmental Science & Technology*, vol. 43, no. 6, pp. 1986–1992, 2009.

[19] C. Pade and M. Guimaraes, "The $CO_2$ uptake of concrete in a 100 year perspective", *Cement and Concrete Research*, vol. 37, no. 9, pp. 1348–1356, 2007.

[20] F. Xi, S. J. Davis, P. Ciais, D. Crawford-Brown, D. Guan, C. Pade, T. Shi, M. Syddall, J. Lv, L. Ji, L. Bing, J. Wang, W. Wei, K. Yang, B. Lagerblad, I. Galan, C. Andrade, Y. Zhang, and Z. Liu, "Substantial global carbon uptake by cement carbonation", *Nature Geoscience*, vol. 9, no. 12, pp. 880–883, 2016.

[21] K. Vance, G. Falzone, I. Pignatelli, M. Bauchy, M. Balonis, and G. Sant, "Direct carbonation of $Ca(OH)_2$ using liquid and supercritical $CO_2$: Implications for carbon-neutral cementation", *Industrial & Engineering Chemistry Research*, vol. 54, no. 36, pp. 8908–8918, 2015.

[22] B. He, Y. Cao, C. E. Romero, H. Bilirgen, N. Sarunac, H. Agarwal, and W. Pan, "Comparison and validation of OHM and SCEM measurements for a full-scale coal-fired power plant", *Chemical Engineering Communications*, vol. 194, no. 12, pp. 1596–1607, 2007.

[23] E. S Rubin and D. G. Nguyen, "Energy requirements of a limestone FGD system", *Journal of the Air Pollution Control Association*, vol. 28, no. 12, pp. 1207–1212, 1978.

[24] J. Katzer, E.J. Moniz, J. Deutch, S. Ansolabehere, J. Beer, et al., "The future of coal: an interdisciplinary MIT study", Tech. Rep. 978-0-615-14092-6, Massachusetts Institute of Technology, Cambridge, MA, 2007.

[25] A. Bahadori, "Estimation of combustion flue gas acid dew point during heat recovery and efficiency gain", *Applied Thermal Engineering*, vol. 31, no. 8, pp. 1457–1462, 2011.

[26] F. H. Verhoff and J. T. Banchero, "Predicting dew points of flue gases", *Chemical Engineering Progress*, vol. 70, no. 8, pp. 71–72, 1974.

[27] R. R. Pierce, "Estimating acid dew points in stack gases", *Chemical Engineering*, vol. 84, no. 8, pp. 125–28, 1977.

[28] B. ZareNezhad and A. Aminian, "A multi-layer feed forward neural network model for accurate prediction of flue gas sulfuric acid dew points in process industries", *Applied Thermal Engineering*, vol. 30, no. 6, pp. 692–696, 2010.

[29] H. Kikkawa, W. Shimohira, T. Nagayasu, M. Kyosawa, Y. Nagai, and S. Kagawa, "Highly-efficient removal of toxic trace elements and particulate matter in flue gas emitted from coal-fired power plants by air quality control system (AQCS)", *Mitsubishi Heavy Industries Technical Review*, vol. 52, no. 2, pp. 89–96, 2015.

[30] N. Noda and H. Makino, "Influence of operating temperature on performance of electrostatic precipitator for pulverized coal combustion boiler", *Advanced Power Technology*, vol. 21, no. 4, pp. 495–499, 2010.

[31] Environmental Protection Agency, "Air pollution fact sheets: Flue gas desulfurization", Tech. Rep. EPA-452/F-03-034, Technology Transfer Network U.S.–Mexico Border Information Center on Air Pollution, 2003.

[32] J. Chang and S. B. Ghorishi, "Simulation and evaluation of elemental mercury concentration increase in flue gas across a wet scrubber", *Environmental Science & Technology*, vol. 37, no. 24, pp. 5763–5766, 2003.

[33] L. E. Shoemaker and J. R. Crum, "Experience in effective application of metallic materials for construction of FGD systems", *Special Metals Corporation*, 2010.

[34] Sargent & Lundy, "Wet flue gas desulfurization technology evaluation", Tech. Rep. 11311-000, National Lime Association, 2003.

[35] R. K. Srivastava and W. Jozewics, "Flue gas desulfurization: The state of the art", *Journal of the Air & Waste Management Associate*, vol. 51, no. 12, pp. 1676–1688, 2001.

[36] Energy Information Administration, "Annual energy review", Tech. Rep. DOE/EIA-0384, U.S. Department of Energy, Washington, D.C., 2011.

[37] S. P. Schweinfurth, "The national coal resource assessment overview, Chapter C: An introduction to coal quality", Tech. Rep. 1625-F, U.S. Department of the Interior, Reston, VA, 2009.

[38] Energy Information Administration, "U.S. coal reserves: an update by heat and sulfur content", Tech. Rep. DOE/EIA-0529(92), U.S. Department of Energy, Washington, D.C., 1993.

[39] Office of Air and Radiation, "Compilation of air pollutant emission factors Volume I: Stationary point and area sources", Tech. Rep. AP-42, Environmental Protection Agency, Research Triangle Park, NC, 1995.

[40] Environmental Protection Agency, "Continuous emissions monitoring system", Database, 2010, "`https://www.epa.gov/emc/emc-continuous-emission-monitoring-systems`".

[41] C. E. V. Atten, A. Saha, L. Slawsky, and C. Russell, "Benchmarking air emissions of the 100 largest electric power producers in the United States", Tech. Rep. (no #), Concord, MA, 2015.

[42] United State Geological Survey, "Minerals yearbook: Cement", Annual report, Department of the Interior, Washington, D.C., 2015.

[43] E. Worrell, L. Price, N. Martin, C. Hendriks, and L. O. Meida, "Carbon dioxide emissions from the global cement industry", *Annual Review of Energy and the Environment*, vol. 26, no. 1, pp. 303–329, 2001.

[44] W. T. Choate, "Energy and emission reduction opportunities for the cement industry", Tech. Rep., BCS Incoporated, Columbia, MD, 2015.

[45] L. Price, A. Hasanbeigi, and N. Zhou, "Increasing energy efficiency and reducing emissions from China's cement kilns: Audit report of two cement plants in Shandong Province, China", Tech. Rep. LBNL-5583E, Lawrence Berkeley National Laboratory, Berkeley, CA, 2011.

[46] B. Wang, G. Falzone, J. Di Filippo, C. Lin, L. Linden, K. Jessup, G. Sant, J. R. De Shazo, R. Kaner, M. Bauchy, and L. Pilon, "NRG Cosia Carbon X-Prize, round 1 submission", XPrize Foundation [Unpublished], 2016.

[47] Energy Information Administration, "Electric power annual 2014", Annual report, U.S. Department of Energy, Washington, D.C., 2014.

[48] H. Daneshvar, R. Prinja, and N. P. Kherani, "Thermophotovoltaics fundamentals, challenges and prospects", *Applied Energy*, vol. 159, pp. 560–575, 2015.

[49] D. Meyer, C. Wong, F. Engel, and S. Krumdieck, "Design and build of 1 kilowatt organic Rankine cycle power generator", Roturua, New Zealand, 2013, 35th New Zealand Geothermal Workshop, pp. 17–20.

[50] G. Pei, J. Li, Y. Li, D. Wang, and J. Ji, "Construction and dynamic test of a small–scale organic Rankine cycle", *Energy*, vol. 36, no. 5, pp. 3215–3223, 2011.

[51] W. Gu, Y. Weng, Y. Wang, and B. Zheng, "Theoretical and experimental investigation of an organic Rankine cycle for a waste heat recovery system", *Proceedings of the Institution of Mechanical Engineers, Part A: Journal of Power and Energy*, vol. 223, no. 5, pp. 523–533, 2009.

[52] S. H. Kang, "Design and experimental study of ORC (organic Rankine cycle) and radial turbine using R245fa working fluid", *Energy*, vol. 41, no. 1, pp. 514–524, 2012.

[53] X. D. Wang, L. Zhao, J. L. Wang, W. Z. Zhang, X. Z. Zhao, and W. Wu, "Performance evaluation of a low–temperature solar Rankine cycle system utilizing R245fa", *Solar Energy*, vol. 84, no. 3, pp. 353–364, 2010.

[54] G. Qiu, Y. Shao, J. Li, H. Liu, and S. B. Riffat, "Experimental investigation of a biomass–fired ORC–based micro–CHP for domestic applications", *Fuel*, vol. 96, pp. 374–382, 2012.

[55] S. Quoilin, M. Van Den Broek, S. Declaye, P. Dewallef, and V. Lemort, "Techno–economic survey of organic Rankine cycle (ORC) systems", *Renewable and Sustainable Energy Reviews*, vol. 22, pp. 168–186, 2013.

[56] M. J. Moran, H. N. Shapiro, D. D. Boettner, and M. B. Bailey, *Fundamentals of Engineering Thermodynamics*, John Wiley & Sons, United States, 2010.

[57] A. I. Papadopoulos, M. Stijepovic, and P. Linke, "On the systematic design and selection of optimal working fluids for organic Rankine cycles", *Applied Thermal Engineering*, vol. 30, no. 6, pp. 760–769, 2010.

[58] U. Drescher and D. Brüggemann, "Fluid selection for the organic Rankine cycle (ORC) in biomass power and heat plants", *Applied Thermal Engineering*, vol. 27, no. 1, pp. 223–228, 2007.

[59] B. Liu, K. Chien, and C. Wang, "Effect of working fluids on organic Rankine cycle for waste heat recovery", *Energy*, vol. 29, no. 8, pp. 1207–1217, 2004.

[60] T Hung, "Waste heat recovery of organic Rankine cycle using dry fluids", *Energy Conversion and Management*, vol. 42, no. 5, pp. 539–553, 2001.

[61] M. Peters, K. Timmerhaus, and R. West, *Plant Design and Economics for Chemical Engineers*, McGraw-Hill Education, Boulder, CO, 2012.

[62] Y. A Çengel, R. H. Turner, J. M. Cimbala, and M. Kanoglu, *Fundamentals of Thermal-Fluid Sciences*, McGraw-Hill, New York, NY, 2005.

[63] E. H. Wang, H. G. Zhang, B. Y. Fan, M. G. Ouyang, Y. Zhao, and Q. H. Mu, "Study of working fluid selection of organic Rankine cycle (ORC) for engine waste heat recovery", *Energy*, vol. 36, no. 5, pp. 3406–3418, 2011.

[64] A. A. Lakew and O. Bolland, "Working fluids for low-temperature heat source", *Applied Thermal Engineering*, vol. 30, no. 10, pp. 1262–1268, 2010.

[65] K. Yang, H. Zhang, Z. Wang, J. Zhang, F. Yang, E. Wang, and B. Yao, "Study of zeotropic mixtures of ORC (organic Rankine cycle) under engine various operating conditions", *Energy*, vol. 58, pp. 494–510, 2013.

[66] S. Quoilin, *Sustainable Energy Conversion Through the Use of Organic Rankine Cycles for Waste Heat Recovery and Solar Applications.*, PhD thesis, University of Liège (Belgium), 2011.

[67] P. Song, M. Wei, L. Shi, Syed N. Danish, and C. Ma, "A review of scroll expanders for organic Rankine cycle systems", *Applied Thermal Engineering*, vol. 75, pp. 54–64, 2015.

[68] J. M. Calm and G. C. Hourahan, "Refrigerant data summary", *Engineered Systems*, vol. 18, no. 11, pp. 74–88, 2001.

[69] E. Cayer, N. Galanis, M. Desilets, H. Nesreddine, and P. Roy, "Analysis of a carbon dioxide transcritical power cycle using a low temperature source", *Applied Energy*, vol. 86, no. 7, pp. 1055–1063, 2009.

[70] E. H. Wang, H. G. Zhang, Y. Zhao, B. Y. Fan, Y. T. Wu, and Q. H. Mu, "Performance analysis of a novel system combining a dual loop organic Rankine cycle (ORC) with a gasoline engine", *Energy*, vol. 43, no. 1, pp. 385–395, 2012.

[71] Y. Chen, P. Lundqvist, A. Johansson, and P. Platell, "A comparative study of the carbon dioxide transcritical power cycle compared with an organic Rankine cycle with r123 as working fluid in waste heat recovery", *Applied Thermal Engineering*, vol. 26, no. 17, pp. 2142–2147, 2006.

[72] Y. Li, M. Du, C. Wu, S. Wu, C. Liu, and J. Xu, "Economical evaluation and optimization of subcritical organic Rankine cycle based on temperature matching analysis", *Energy*, vol. 68, pp. 238–247, 2014.

[73] P. Grassmann, *Physical Principles of Chemical Engineering: International Series of Monographs in Chemical Engineering*, vol. 12, Elsevier, 2013.

[74] R. Turton, R. C. Bailie, W. B. Whiting, and J. A. Shaeiwitz, *Analysis, synthesis, and Design of Chemical Processes*, Pearson Education, 2008.

[75] H. P. Loh, J. Lyons, and C. W. White, "Process equipment cost estimation", Tech. Rep. DOE/NETL-2002/1169, National Energy Technology Lab, Morgantown, WV, 2002.

[76] R. Eggers, *Industrial High Pressure Applications: Processes, Equipment, and Safety*, John Wiley & Sons, 2012.

[77] B. Wang, "Discussion of modeling two stage compression for the X-Prize submission", April 2016, Private communication.